Immunopathology in human lymphoedema

Maria Paula Mempin
42133211
Australian School of Advanced Medicine, Macquarie University

A thesis submitted for the partial fulfillment of the requirements for the degree of Master of Research in Advanced Medicine

Supervisor
Dr. Lisa Sedger[1]
[1]Cancer Institute, Macquarie University, Australian School of Advanced Medicine, North Ryde, NSW, Australia

Keywords: Lymphoedema, adipose tissue, collagen, fibrosis, macrophages, blood endothelial cells, lymphatic endothelial cells

Main text word count: 10759
Abstract character count (no spaces): 1562
Number of figures: 23
Number of tables: 3

Declaration of Originality

I certify that the work in this thesis entitled “Immunopathology in human lymphoedema” has not previously been submitted for a degree nor has it been submitted as part of requirements for a degree to any other university or institution other than Macquarie University.

I also certify that the thesis is an original piece of research and it has been written by me. Any help and assistance that I have received in my research work and the preparation of the thesis itself have been appropriately acknowledged.

In addition, I certify that all information sources and literature used are indicated in the thesis. The research presented in this thesis was approved by Macquarie University Ethics Review Committee, reference number: 5201300315

Signature

Maria Paula Mempin

2. Abstract

Lymphoedema is a condition of abnormal tissue swelling resulting from failure of lymph drainage. The condition is often chronic and it frequently results in the accumulation of adipose tissue (AT) within the affected region. The mechanisms underlying AT formation in lymphoedema have not been determined. This research therefore aims to characterize the AT of patients with lymphoedema. Liposuction tissue samples were obtained from lymphoedema patients' limbs (4 arms, 4 legs) and from limbs of healthy individuals undergoing cosmetic liposuction surgery (3 arms, 4 legs). AT tissue samples were fixed in neutral buffered formalin and processed for histological analysis, including hematoxylin and eosin, Milligan's trichrome, or picrosirius red staining. Image analysis was performed to determine the mean adipocyte cell number, size, tissue fibrosity, and the degree of collagen deposition. Immunohistochemical analyses was also performed, using antibodies specific to lymphatic endothelial cells (podoplanin), blood vascular endothelial cells (CD31), and macrophages (HAM56), to determine the relative location of perivascular collagen and the identity of macrophage-like cells. Histological analysis of lymphoedema AT revealed abundant collagen, especially type III collagen, and perivascular fibrosis. Overall, adipocyte cell number, size, and the extent of collagen content were found to be similar in lymphoedema and normal AT. Using immunohistochemistry, we detected CD31 expression in lymphoedema and normal AT, and this occurred in areas of collagen deposition. Unfortunately, no positive staining for podoplanin and HAM56 were detected in either lymphoedema or normal AT. Taken together, this research provides important information into the etiopathology of this chronic and debilitating condition.

3. Conflict of Interest Statement

We declare that there are no conflicts of interest and this research was conducted in the absence of any commercial or financial relationships that could be construed as a potential conflict of interest.

Table of Contents

List of Figures

List of Figures (continued)

List of Tables

4. Introduction

Lymphoedema is a progressive chronic condition of the lymphatic system, in which there is excessive build up of protein-rich interstitial fluid in body tissues causing abnormal swelling (Szuba and Rockson, 1998; Rockson, 2001; Warren et al., 2007). Lymphatic channels primarily regulate the flow of fluid in the interstitium (Ellis, 2006). Under normal conditions, venous capillaries reabsorb 90% of the fluid in the interstitium, while the remaining fluid is transported by the lymphatics as "lymph" (Warren et al., 2007). Thus, the lymphatic system plays an important role in maintaining fluid balance and tissue homeostasis, a balance that is disrupted in lymphoedema due to lymphatic insufficiency and inadequate lymph transport (Szuba and Rockson, 1998; Rockson, 2001; Warren et al., 2007). Chronic interstitial fluid accumulation has been shown to promote lipogenesis and an accumulation of subcutaneous adipose tissue (AT), leading to increased fibrocyte activation and connective tissue overgrowth (Gaffney and Casley-Smith, 1981; Šmahel, 1986; Ryan, 1995).

Lymphoedema is generally classified as either primary or secondary. Primary lymphoedema has a genetic origin, which usually manifests itself from birth (Milroy's disease) (Milroy, 1892) or at the onset of puberty (Meige's disease) (Meige, 1898; Warren et al., 2007), and is usually due to a congenital malformation of the lymphatic system. Primary lymphoedema has been associated with mutations in genes important for the growth and development of the lymphatic vasculature (lymphangiogenesis). For example, mutations in genes encoding the vascular endothelial growth factor receptor-3 (*VEGFR-3*), important for normal lymphatic vascular function; Forkhead transcription factor (*FOXC2*), expressed on developing lymphatic cells; and transcription factor *SOX18* (Sry-type high-mobility group [HMG] box), important for blood vascular development and lymphatic development, have all been identified as being associated with primary lymphoedema (Fang et al., 2000; Irrthum et al., 2000; Karkkainen et al., 2000; Bell et al., 2001; Finegold et al., 2001; Irrthum et al., 2003). At birth, about one person in every 6000 will develop primary lymphoedema (Warren et al., 2007).

The most prevalent form of lymphoedema is secondary, or acquired lymphoedema, which develops following damage to the lymphatic vessels and/or lymph nodes, usually as a consequence of cancer treatment (Hinrichs et al., 2004; Ozaslan and Kuru, 2004; Gordon and Mortimer, 2007). Once damage has occurred to the lymphatic system, lymph fluid transport capacity is permanently diminished in the affected region, thereby predisposing that region to lymphoedema. In Australia, secondary lymphoedema is estimated to occur in up to 52% of breast cancer patients if treatment requires axillary surgery to remove lymph nodes and/or radiation therapy (DiSipio et al., 2013). Whether primary or secondary in origin, without intervention, chronic lymphoedema leads to progressive swelling and AT accumulation.

At present, there is no cure for lymphoedema, and current treatments are limited to manual lymphatic drainage, massage, use of compression garments, compression bandaging, and skin care to minimize lymphoedema-associated limb swelling and risk of infection (Foldi, 1998; Rockson, 2001; Brorson, 2003). However, these approaches merely "manage" the condition, and over time the swelling still persists and generally worsens. Nevertheless, increased AT deposition has led to the innovative use of liposuction surgery for the treatment of lymphoedema, providing an instant reduction in excess limb volume (Brorson and Svensson, 1998; Brorson, 2003). Of note, however, liposuction surgery is not a cure for lymphoedema, and patients must continue to wear their compression garments if they are to achieve the long-term benefits of surgery. Although no amount of compression can reduce the fat tissue.

Thus, there is need to better understand the pathophysiology of lymphoedema and find a cure for lymphoedema.

At present, little is known about AT development in lymphoedema. However, given (i) the accumulation of AT that occurs in the edematous regions of many lymphoedema patients (Gaffney and Casley-Smith, 1981; Šmahel, 1986; Ryan, 1995), (ii) the ability of lymph to promote the differentiation of pre-adipocytes to mature adipocytes *in vitro* (Nougues et al., 1988), (iii) the fact that lymph nodes are normally embedded in AT, and (iv) that subcutaneous AT lies in close proximity to the dermal lymphatic vasculature (Wang and Oliver, 2010), suggests that there exists a close relationship between lymphatic function and adipocyte metabolism.

AT is a complex, essential, and highly active metabolic and endocrine organ (Ahima and Flier, 2000; Frühbeck et al., 2001). White adipose tissue (WAT) is composed of mature adipocytes (fat cells), precursors (pre-adipocytes), and fibroblasts (Ailhaud, 2001; Katz, 2002; Cristancho and Lazar, 2011). It is also highly vascularized (Ailhaud, 2001; Katz, 2002; Cristancho and Lazar, 2011), where blood and lymphatic vessels consist of endothelial cells, pericytes, and smooth muscle cells (Ailhaud et al., 1992). The adipocytes themselves differentiate from mesenchymal stem cells (MSCs) in a process known as adipogenesis (Gesta et al., 2007). This is a highly controlled process involving numerous transcription factors regulating gene expression, ultimately leading to the differentiation of pre-adipocytes into large lipid-filled adipocytes (Rosen and MacDougald, 2006). Mature adipocytes are the predominant cell type in AT. Normal AT also constitutively contains a number of leukocytes, including an abundant population of multi-potent stem cells (Zuk et al., 2001; Zuk et al., 2002). Recently it has also become clear that AT contains macrophages (Mφ) (Aron-Wisnewsky et al., 2009; Divoux et al., 2010; Fjeldborg et al., 2014).

The mechanism(s) of AT accumulation due to lymphatic vascular dysfunction have not yet been determined. However, insights into a potential mechanism are suggested by studies in mice haploinsufficient for *Prox1*, a gene encoding a homeobox transcription factor important for lymphatic vascular development (Harvey et al., 2005). Targeted inactivation of a single allele of *Prox1* promotes lymphatic vascular defects that cause adult-onset obesity (Harvey et al., 2005), where a consistent association was observed between the degree of lymphatic disorganization, and the degree of AT accumulation. In addition, abnormal or excessive lymph leakage occurred in areas abundant in disorganized lymphatic vessels, particularly the mesentery (Harvey et al., 2005).

To investigate whether lymphatic vascular disorganization and leakage were linked with AT accumulation, mouse 3T3-L1 pre-adipocytes were cultured with lymph collected from newborn *Prox1*$^{+/-}$ pups – since it has long been known that lymph and chylomicrons stimulates the differentiation of rabbit pre-adipocytes *in vitro* (Nougues et al., 1988). Indeed, lymph from newborn *Prox1*$^{+/-}$ pups promotes 3T3-L1 adipocyte differentiation (Harvey et al., 2005). Thus, disruption of the lymphatic vasculature promotes the accumulation of AT in lymphatic-rich regions due in part to increased lipid storage in adipocytes and increased differentiation of pre-adipocytes to mature adipocytes (Harvey et al., 2005).

Interestingly, AT accumulation in *Prox1*$^{+/-}$ mice is also associated with an increased number of LYVE-1 (lymphatic vessel endothelial hyaluronan receptor-1) positive Mφ in the mesentery (Harvey et al., 2005). This finding is particularly interesting because numerous observations suggest that inflammatory factors, secreted directly from adipocytes and AT-

derived Mφ, may underlie metabolic diseases such as obesity. In fact, in obese humans, as well as animal models of obesity, there are often increased numbers of Mφ in the AT, which produce a wide range of cytokines and chemical mediators that drive a pro-inflammatory response (Weisberg et al., 2003; Xu et al., 2003; Dandona et al., 2004; Cancello et al., 2005). For example, Mφ are known to produce high quantities of interleukin-1β (IL-1β) (Lagathu et al., 2006), while adipocytes produce adipokines such as adiponectin, leptin and resistin (Bełtowski, 2003). Both cell types are thought to contribute to the production of pro-inflammatory cytokines, such as tumor necrosis factor (TNF) and interleukin-6 (IL-6) (Weisberg et al., 2003; Xu et al., 2003). To date however, the AT that develops in lymphoedema is essentially uncharacterized. It is not known, for example, whether Mφ are present in normal and lymphoedema AT, and if they play a similar role to AT Mφ in obesity.

Much of what is "known" about the processes of AT generation have come from studies investigating the processes of adipogenesis or the pathology of obesity. AT can respond rapidly and dynamically to alterations in nutrient deprivation and excess, through adipocyte hypertrophy (an increase in adipocyte volume) and hyperplasia (an increase in adipocyte cell number) (Halberg et al., 2008; Khan et al., 2009; Sun et al., 2011). In this sense AT fulfills a major role in whole body energy homeostasis (Sun et al., 2011). AT modeling is an ongoing process that is pathologically accelerated in the obese state, and thus, features such as reduced angiogenic remodeling, extracellular matrix (ECM) overproduction, increased connective fiber content, a heightened state of immune cell infiltration and subsequent pro-inflammatory responses prevail in AT in obesity (Halberg et al., 2008; Khan et al., 2009; Rutkowski et al., 2009).

To re-iterate, there have been no published studies to date describing the AT that develops in chronic lymphoedema. Since clinicians at Macquarie University Hospital (MUH) are now performing liposuction surgery for chronic non-pitting lymphoedema, there is an opportunity to examine the AT removed through surgical liposuction of lymphoedema patients. Therefore, this research aims to characterize the AT of patients with lymphoedema, including adipocyte cell number, adipocyte size, tissue fibrosity, collagen content, and the presence of macrophage-like cells. We hypothesize~~d~~ that lymphoedema patients will display an increase in adipocyte cell number and in adipocyte size compared to AT from healthy individuals, and therefore perform a careful histological examination of lymphoedema and normal AT obtained by liposuction surgery. An immunohistochemical (IHC) analysis is also undertaken.

5. Materials and methods

5.1 Subjects

Subcutaneous AT was obtained by surgical liposuction from the arms (n = 5) and legs (n = 4) of patients with primary and secondary lymphoedema. Lymphoedema AT was obtained fresh from the operating room of Macquarie University Hospital (MUH) in 2 L disposable collection bags (Figure 1), transported to the laboratory, and processed immediately. In addition, subcutaneous AT was obtained from the arms (n = 3) and legs (n = 4) of healthy individuals undergoing cosmetic liposuction surgery, which was kindly provided by Dr. Daniel Lanzer (Dr. Lanzer Dermatology, Malvern, Melbourne). Normal AT was obtained fresh from the operating room of Dr. Lanzer's cosmetic surgery clinic in 2 L disposable collection bags, transported to the laboratory in a bio bottle enclosed with gel cold packs by same-day or overnight courier, and processed immediately upon arrival.

Figure 1. Adipose tissue removed by liposuction surgery from the leg of a secondary lymphoedema patient.

5.2 Histopathology of adipose tissue

For each AT patient sample, random aliquots of AT were taken directly from the collection bags and put into tissue processing cassettes (Leica Biosystems, North Ryde, New South Wales). The tissue cassettes were immersed in 10% neutral buffered formalin (Fronine, Riverton, New South Wales), and after 24-48 hours of fixation, tissues were taken to the Histopathology Laboratory, Department of Pathology, The University of Sydney for paraffin embedding and processing for histological analysis. AT were treated with xylene and rehydrated through a graded alcohol series. AT were then infiltrated with molten paraffin wax, by heating the tissue to the melting point of wax (50-60˚C). Paraffin-embedded AT were cut in 5 µm thick sections on a microtome and collected onto 3-aminopropyltriethoxy-silane coated slides. The slides were dried in an oven at 37-42˚C and stained with Harris' hematoxylin and eosin (H&E), Milligan's trichrome (MT), and picrosirius red (PSR) as previously described (Gray, 1954; Drury and Wallington, 1967; Kiernan, 1999).

5.3 Visualization and image acquisition

Bright field images of AT, stained with H&E, MT and PSR, were obtained on a Olympus BX51 microscope (Olympus, Notting Hill, Victoria) equipped to carry out bright field and epifluorescence microscopy, at 10X, 20X or 40X magnification. Images were acquired with a Olympus DP70 CCD camera (Olympus) at 1360 x 1024 pixels and RGB-color format controlled with Olympus cellSens imaging software (Olympus, version 1.0). Light settings were not fixed throughout the digital acquisition of all images. Collagen birefringence was assessed in polarized light after the tissue sections were stained with PSR, using a Olympus microscope equipped with polarized light optics, with kind assistance from Dr. Suha Kilani (IVF Australia, Maroubra, New South Wales). Images were acquired with a black and white camera (Olympus). When polarization microscopy is used, type I collagen fibers appear orange to red, whereas the thinner type III collagen fibers appear yellow to green (Junqueira et al., 1979). The birefringence is highly specific for collagen and represents an index of the organization of collagen fibers (Junqueira et al., 1979). Images were analysed using ImageJ processing software (National Institutes of Health (NIH), version 2.0, Maryland, USA). Images were spatially calibrated from pixel units to micron (μm) units using a 1.02 μm/pixel ratio obtained through cellSens software (Olympus).

5.4 Measurement of adipocyte cell number and size

Adipocyte cell number and size was assessed in AT sections from primary lymphoedema arm (n = 1), secondary lymphoedema arm (n = 4) and leg (n = 4), and normal arm (n = 3) and leg (n = 4). For each MT stained section, bright field images were randomly acquired from six different fields at 10X magnification. Epifluorescent images of the same MT stained sections were also randomly acquired from six different fields per section at 10X magnification. A single long pass filter in the red wavelength range with an excitation bandpass of 530-550 nm and emission at 575 nm was used (Olympus).

To calculate adipocyte cell number and size, epifluorescent images were converted to 8-bit images using ImageJ software (NIH). Grayscale images were then converted to binary images (having only two pixel values of 0 for white and 255 for black) using the “Threshold” command. Threshold analysis is an image segmentation technique that removes all artifacts and isolates features or “particles” of interest. A threshold was individually defined for each image by adjusting the lower and upper bounds of the threshold limit to eliminate background noise and still allow discrimination of AT morphology. The particles (or adipocytes) were then counted and measured individually using the “Analyze Particles” command, setting a 500-infinity μm^2 range to exclude any remaining artifacts or non-adipocyte cells that were not an object of interest in the image. A “Exclude on Edges” function was selected to exclude particles that are on the edge of the image; and a “Show Outlines” function was selected to display the image as an outlined cartoon, with each particle numbered to give corresponding count and area measurements. To confirm that the detected particle was an adipocyte cell, the outlined cartoon image was assessed visually by comparing it to its corresponding MT stained image. An adipocyte was defined by regularly round MT stained cells without plasma membrane disruption. The area of each cell meeting this inclusion criterion was averaged into a single measurement in each of the six different fields per AT section. The six fields in each AT section were then averaged into a single measurement. Adipocyte cell size in each liposuction-derived AT sample was expressed as the mean adipocyte size (μm^2).

The adipocyte cell number in each field of view was calculated by dividing the adipocyte cell count by the total area of the tissue. The area of the tissue was determined using the “Polygon Tool” function to manually trace an outline around the total area of the tissue, excluding

particles that are on the edge of the image. A “Create Mask” command was then used to create a “mask” of the trace that could be thresholded and converted to an outlined cartoon image to obtain a single area measurement. The total number of adipocytes per tissue area was calculated in each of the six different fields per AT section, and averaged into a single measurement. Mean adipocyte cell number was normalized to the mean number of adipocytes per 1 mm^2 area. Therefore, measurements of mean adipocyte cell number and mean adipocyte size was determined for each liposuction-derived AT sample from lymphoedema arms (n = 5) and legs (n = 4), and normal arms (n = 3) and legs (n = 4).

The proportion of non-adipocyte cells was also assessed in AT sections from primary lymphoedema arm (n = 1), secondary lymphoedema arm (n = 4) and leg (n = 4), and normal arm (n = 3) and leg (n = 4). To calculate the proportion of non-adipocyte cells, the sum of the area per adipocyte was subtracted from the total area of the tissue (as determined above). Because some AT samples contained areas with collagen and blood vessels, area measurements for collagen and blood vessels were made by thresholding the image and converting it to an outlined cartoon image to obtain their area measurements. These measurements were then also subtracted from the total area of the tissue.

5.5 Measurement of collagen content

The extent of collagen present was assessed in AT sections from primary lymphoedema arm (n = 1), secondary lymphoedema arm (n = 4) and leg (n = 4), and normal arm (n = 3) and leg (n = 4). For each MT stained section, bright field images that covered the entire section of AT were obtained at 10X magnification, in order to achieve a representative assessment of collagen content in AT samples. ImageJ’s “Stitching” plugin (Preibisch et al., 2009) was used to stitch the bright field images together to create large-format images that covered the entire section of AT.

To determine the proportion of collagen content, each stitched image was first separated into three fluorescent color-isolated images using ImageJ’s “Colour Deconvolution” command according to previously described methods (Ruifrok and Johnston, 2001). The fluorescent color-isolated image showing only collagen areas (green or red) was then thresholded and converted to an outlined cartoon image, with each collagen area numbered to give corresponding area measurements. To calculate the percent collagen content per AT area, again, an outline was manually traced around the total area of the tissue, excluding particles that are on the edge of the image. A ‘mask’ of this trace was then created, then thresholded, and converted to an outlined cartoon image to give a single area measurement. The area of collagen content was expressed as percentage of the total AT area measured. Collagen content was normalized to the proportion of collagen per 1 mm^2 area. Therefore, measurements of the proportion of collagen content was determined for each liposuction-derived AT sample from lymphoedema arms (n = 5) and legs (n = 4), and normal arms (n = 3) and legs (n = 4).

5.6 Immunohistochemical analysis of adipose tissue

Immunohistochemistry (IHC) is used to localize specific antigens or proteins in tissue sections with labelled antibodies based on antigen-antibody interactions. The immune reactive products are then visualized by a marker such as enzyme or fluorescent dye. IHC was used to determine the relative location of perivascular collagen and the identity of macrophage-like cells in lymphoedema AT.

Formalin-fixed, paraffin-embedded AT sections were examined by IHC using primary mouse monoclonal antibodies specific to lymphatic endothelial cells (podoplanin) (DAKO, Glostrup, Denmark), blood vascular endothelial cells (CD31) (DAKO), smooth muscle actin (DAKO), and macrophages (HAM56) (GeneTex, Irvine, USA). Primary mouse antibodies were detected using a DAKO EnVisionTM FLEX Mini Kit, high pH (catalog no. K8024, DAKO).

For antibody staining, tissue sections were deparaffinised in two successive baths of xylene (Fronine, Riverton, New South Wales) for 10 min each and rehydrated through graded alcohol treatment, starting with 100% ethanol (Chem-Supply, Gillman, South Australia) (two changes, 5 min each), 95% ethanol (two changes, 5 min each), 70% ethanol for 5 min, and dH_2O for 5 min to adequately remove ethanol. Antigen retrieval was performed through the use of EnVisionTM FLEX target retrieval solution, high pH (DAKO). A 2 L glass beaker containing 500 ml of dH_2O was heated to 100˚C on a hot plate. Racked slides were placed in a slide-staining dish (ProSciTech, Kirwan, Queensland) containing the target retrieval solution and covered with a lid. The staining dish was then placed in the pre-heated water bath and incubated for 25 min at 100˚C. Following antigen retrieval, the staining dish was removed from the water bath and the slides allowed to cool in the target retrieval solution for 20 min at room temperature. Sections were then washed with dH_2O for 5 min and then with EnVisionTM FLEX wash buffer (DAKO) for 5 min. Endogenous peroxidase was blocked by incubating sections in 200 µl of EnVisionTM FLEX peroxidase-blocking reagent (DAKO) for 5 min at room temperature. Sections were washed twice with wash buffer (DAKO) for 5 min each and surrounded with a hydrophobic barrier using commercially available candle wax. Sections were incubated with 200 µl of the specific primary antibody for 1 hr at room temperature. Primary antibodies were diluted in EnVisionTM FLEX antibody diluent (DAKO) at a concentration of 1:100. Sections were then thoroughly rinsed in wash buffer (DAKO), followed by incubation for 30 min at room temperature with 200 µl of EnVisionTM FLEX polymer-HRP secondary antibody (DAKO). Sections were then thoroughly rinsed in wash buffer (DAKO) and developed with chromogen 3,3'-diaminobenzidine (DAB) (DAKO). DAB chromogen working solution was prepared by mixing thoroughly one drop EnVisionTM FLEX DAB+ chromogen per 1 ml EnVisionTM FLEX substrate buffer (DAKO), and applied to the sections for 10 min with the intensity of the tissue staining monitored under a Olympus CK40 light microscope (Olympus). Sections were then rinsed well with dH_2O and counterstained with 10% wt/vol fast green FCF in glacial acetic acid for 15 sec.

Sections were dehydrated with increasing gradients of ethanols using 95% ethanol (two changes, 10 sec each), 100% ethanol (Chem-Supply) (two changes, 10 sec each) and xylene (Fronine) (two changes, 10 sec each), and coverslipped with Vectamount non-aqueous mounting medium (Vector Laboratories, Burlingame, USA). Negative controls for non-specific staining excluded the addition of the primary antibody, which was replaced by normal mouse IgG or IgM (EXBIO, Praha, Czech Republic). Positive controls of tissues, including liver, colon, and spleen, known to contain the antigen of interest were included to test that all reagents were performing as expected. The positive control sections, kindly provided by Mr. Rowan Ikin (Kolling Institute, St Leonards, New South Wales). were fixed and embedded in the same manner as the AT sections.

Bright field images of the IHC staining were obtained on a Olympus BX51 microscope (Olympus) at 10X, 20X or 40X magnification. Again, images were acquired with a Olympus

DP70 CCD camera (Olympus) at 1360 x 1024 pixels and RGB-color format controlled with Olympus cellSens imaging software (Olympus), and processed using ImageJ software (NIH).

5.7 Statistical analysis

Statistical analyses were performed using Prism6 (GraphPad Software Inc., San Diego, USA). The normality of the data distribution was tested first with the normality probability plots test using Minitab 17.0 statistical software (Minitab, State College, USA). The data are presented as mean $\pm$ standard deviation (SD) for lymphoedema AT and normal AT. Student's two-sample t-tests were used to compare mean adipocyte number, mean adipocyte size, proportion of collagen content, and proportion of non-adipocyte cells among lymphoedema arm AT and normal arm AT, and among lymphoedema leg AT and normal leg AT. Differences were considered statistically significant if the *p* value was less than 0.05.

6. Results

6.1 Liposuction surgery reduces limb volume

Limb volume (mL) in unaffected and lymphoedematous (affected) limbs was measured in patients with primary (n=1) and secondary lymphoedema (n=8) at liposuction surgery and at a six-month follow-up assessment using L-Dex. Mean pre-operative limb volume was higher in the affected arm (3803.6 $\pm$ 864.3 mL) compared with the unaffected arm (2641.2 $\pm$ 538.1 mL) in all patients (Figure 2B). Similarly, mean pre-operative edema volume was higher in the affected leg (10825.5 $\pm$ 1498.3 mL) compared with the unaffected leg (7712.25 $\pm$ 1260.7 mL) in all patients (Figure 2C). Liposuction surgery removed the excess volume (fat and fluid) from affected limbs. This meant that by six-months after surgery, there was a significant reduction in mean limb volume in all treated patients ($P < 0.05$), which was now approximately equal to the unaffected limb (Figure 2B, 2C).

6.2 Histological analysis of lymphedema liposuction-derived AT reveals abundant collagen and perivascular fibrosis

Due to the minimal knowledge about the composition and pathology of the AT produced in lymphoedema, liposuction-derived AT samples from lymphoedema patients (n=9) were examined. AT biopsy sections were stained with hematoxylin and eosin (H&E), Milligan's trichrome (MT), and picrosirius red (PSR) for histological analysis using standard light microscopy. Lymphoedema AT showed adipocyte hypertrophy as judged by analysis of adipocyte size (Figure 7). H&E staining also revealed extensive connective tissue, especially around vessels and extending throughout the tissue (Figure 3A(ii,iii), 3B(ii,iii)). Within the connective tissue regions, there were many leukocyte-like cells that morphologically resemble macrophages (Mφ) (Figure 3A(ii,iii), 3B(ii,iii)). MT and PSR staining for collagen revealed collagen fibers as the primary component of the connective tissue (Figure 3A(iv,v), 3B(iv,v)). PSR polarization microscopy was performed for visualization of collagen fibers of different thicknesses with autofluorescence. Type I collagen fibers are orange to red, whereas the thinner type III collagen fibers appear yellow to green (Junqueira et al., 1979). Polarized light microscopy revealed a prevalence of green fibers in lymphoedema AT corresponding with type III collagen (Figure 3A(vi), 3B(vi); image obtained with black and white camera).

6.3 Adipose cell number and size is similar in lymphoedema and normal AT

To determine whether adiposity in lymphoedema parallels the normal processes of adipogenesis, or obesity, adipose cell number and size were assessed in lymphoedema AT (n=9) and compared to the AT of patients having liposuction for non-medical (cosmetic) reasons (n=7). Using ImageJ processing software, we developed a microscopic image analysis method to estimate adipocyte cell number and estimate the average area per adipocyte (Figure 4). Epifluorescent images of the AT samples (n=16) (Figure 4(ii)) were converted to a grayscale image and thresholded to segment the image into features of interest. To calculate adipocyte cell number and area per adipocyte, the thresholded image was converted to an outlined cartoon image, with each segmented feature numbered (Figure 4(iii)) to give corresponding count and area measurements (Table 2). To determine the total number of adipocytes per area of the AT sample, an outline was manually traced around the total area of the tissue (Figure 4(iv)). A 'mask' of this trace was then created to allow the image to be thresholded (Figure 4(v)) and converted to an outlined cartoon image (Figure 4(vi)) to give a single area measurement (Table 2).

Table 1. Lymphoedema patients' diagnosis and lymphoedema experience.

Patient ID[1]	Sex: M/F	Arm or Leg	Original Diagnosis and Date	Original Treatment	Years[2]	Lymphoedema Treatment Prior to Liposuction Surgery
2013_004_MM	F	Arm	Primary lymphoedema; 2011		2	Compression garment, massage
2013_005_PE	F	Arm	Breast cancer; 1982	Mastectomy, axillary clearance, chemotherapy, and radiotherapy	29	Compression garment, massage
2013_006_TE	F	Leg	N/A	N/A		
2013_008_HM	F	Arm	Breast Cancer; 2010	Mastectomy, axillary clearance, chemotherapy, radiotherapy, and hormone therapy	2	Compression garment, massage
2013_009_AD	F	Leg	Ovarian cancer; 1992	Radical hysterectomy, chemotherapy, and radiotherapy	>15	Compression garment, massage
2013_010_LK	F	Leg	Uterine cancer; 1997	Radical hysterectomy	12	Compression garment, massage
2013_011_MN	F	Leg				Compression garment, massage
2013_012_XX			N/A	N/A		N/A
2014_013_LS	F	Leg	Ovarian cancer; 1989	Oophorectomy and chemotherapy	10	Compression garment, massage, laser, bandaging
2014_014_ER	F	Arm	Breast cancer; 1997	Mastectomy and axillary clearance	15	Compression garment, massage, laser, bandaging
2014_015_BG	F	Arm	Breast cancer; 2002	Mastectomy, axillary clearance, radiotherapy, chemotherapy, and hormone therapy	11	Compression garment, massage, laser, bandaging
2014_016_SP	F	Arm	Breast cancer; 2007	Mastectomy, axillary clearance, radiotherapy, chemotherapy, and hormone therapy	6	Compression garment, massage, laser, bandaging
2014_017_AM	F	Leg	NHL cancer; 1997	Excision biopsy of lymph nodes and chemotherapy	14	Bandaging, compression garments, massage
2014_018_CVR	F	Arm	Breast cancer; 2009	Mastectomy, axillary clearance, radiotherapy, chemotherapy, and hormone therapy	3	Bandaging, compression garments, massage
2014_019_CA	F	Arm	Breast cancer; 2008	Lumpectomy, axillary clearance, radiotherapy, chemotherapy, and hormone therapy	5	Compression garment, laser therapy, bandaging
2014_020_BF	F	Leg	Desmoid cancer; 1983	Bilateral oophorectomy, removal of psoas muscle, radiotherapy, chemotherapy, and excision biopsy of nodes	26	Compression garment, laser, massage, bandaging
2014_021_MD	F	Leg	2007 – spider bite (trauma)	N/A	7	Bandaging, massage
2014_022_MP	F	Arm	Breast cancer; 2008	Bilateral mastectomy, axillary clearance, radiotherapy, chemotherapy, and hormone therapy	3	Compression garments, bandaging

[1] Patients consenting to participate in the Macquarie University Human Research Ethics Committee approved study.
[2] Patients clinically diagnosed or self-reported years of living with lymphoedema symptoms, e.g. limb swelling etc.

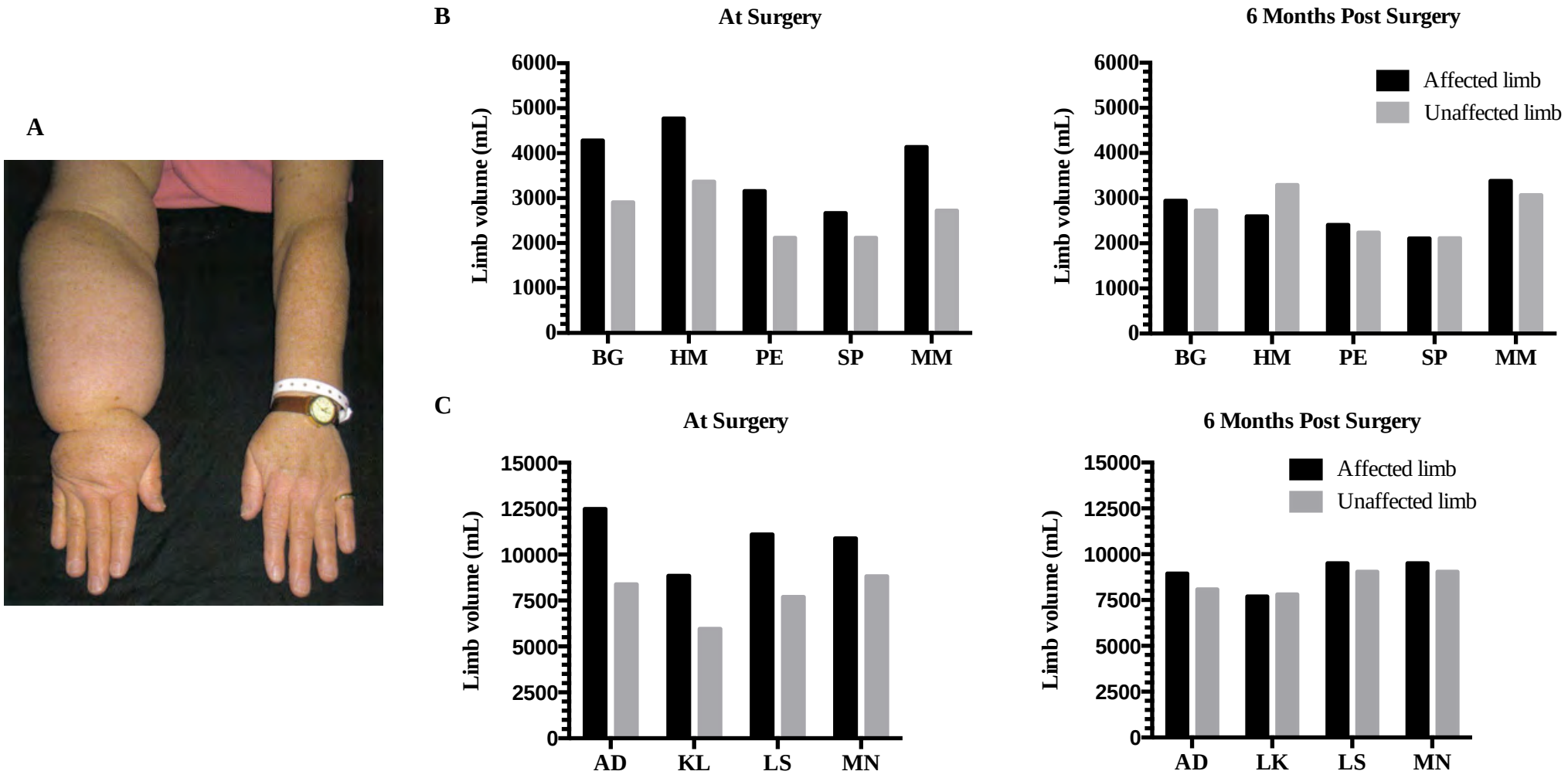

Figure 2. (A) Arm lymphoedema. Limb volume (mL) of lymphoedema patients at time of surgery and 6-months post surgery in **(B)** the affected and unaffected arm, and **(C)** the affected and unaffected leg.

A Lymphoedema arm adipose tissue

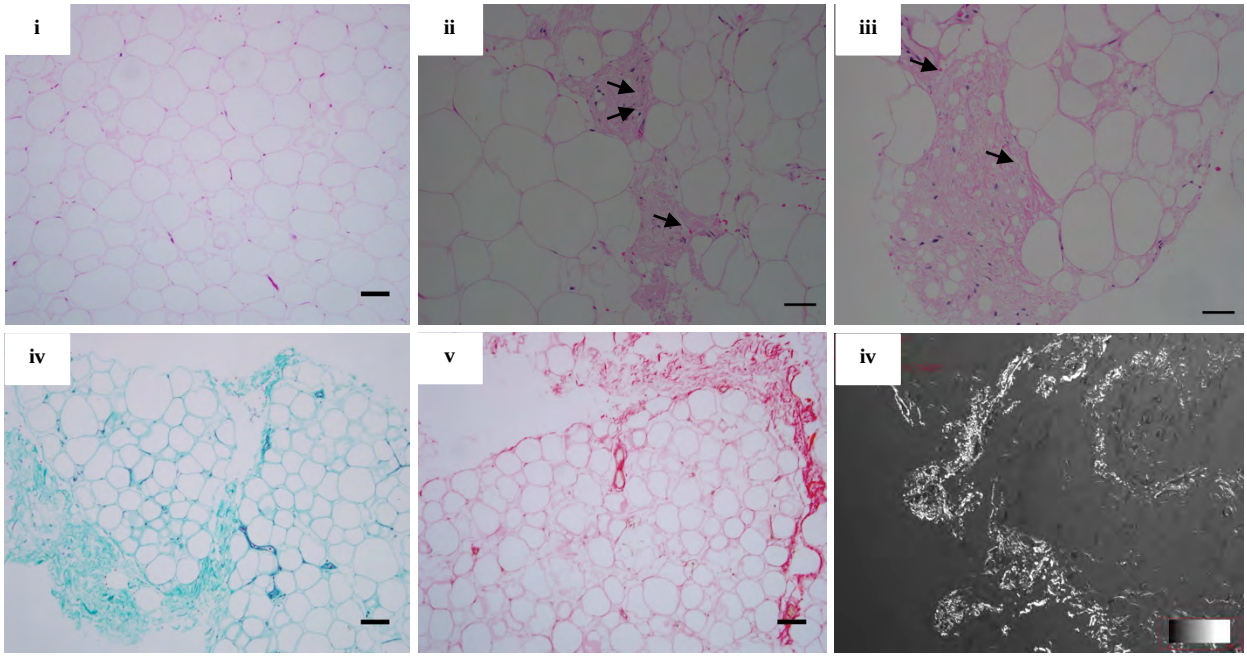

B Lymphoedema leg adipose tissue

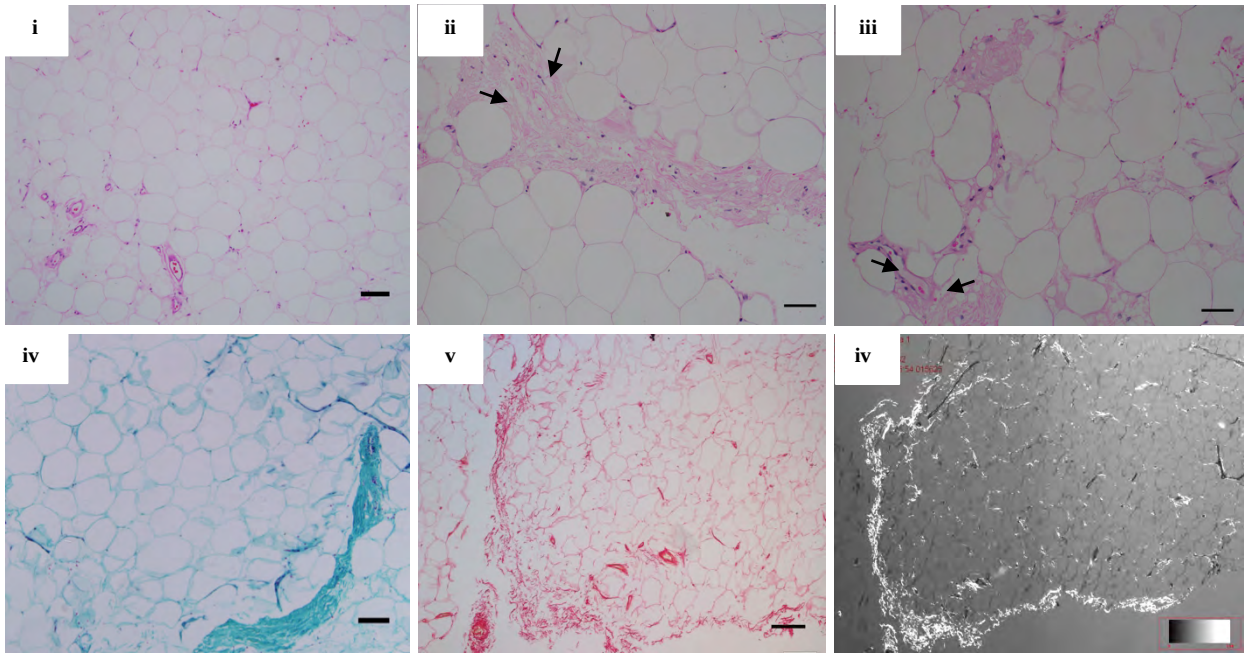

Figure 3. Histology assessments of **(A)** arm lymphoedema AT and **(B)** leg lymphoedema AT at 10X magnification. AT were stained with H&E (i-iii), MT (iv) and PSR (v). PSR polarization microscopy was performed for visualization of collagen fibers (vi). Arrows show accumulation of fibrosis around vessels **(A)**(ii,iii), **(B)**(ii,iii). Scale bars represent 100 µm.

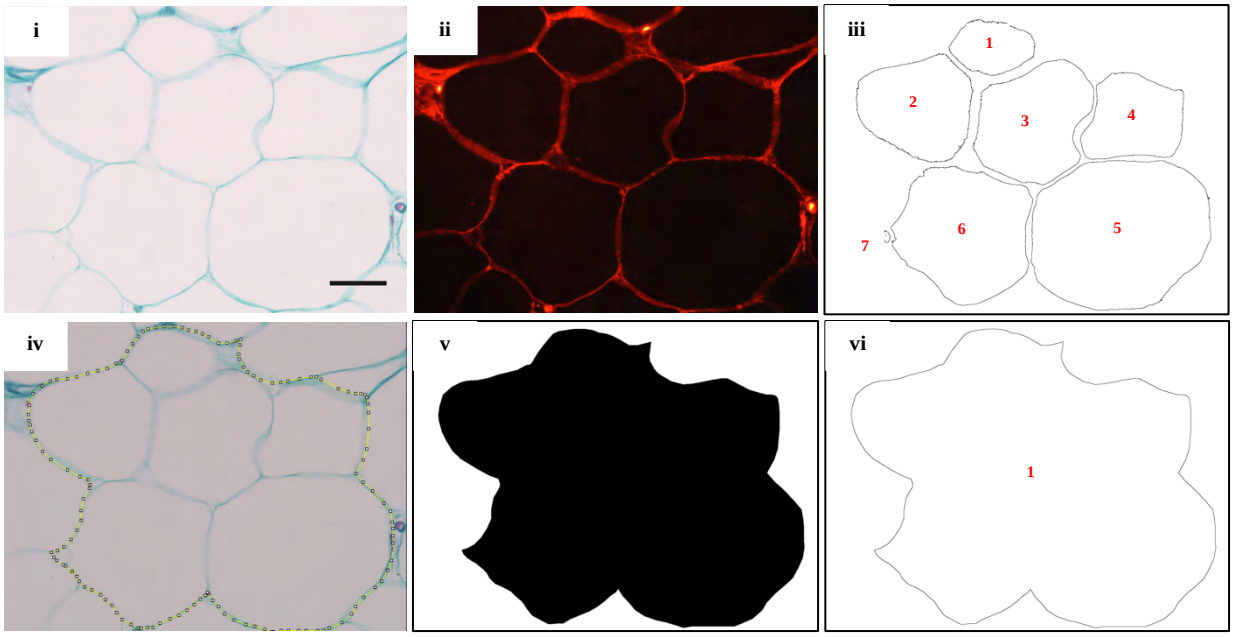

Figure 4. Image analysis method used to quantify adipocyte cell number and size. (i) MT stained AT viewed under light microscopy at 40X magnification; (ii) epifluorescent image at 40X magnification; (iii) outlined cartoon image showing numbered adipocytes that correspond to count and area measurements; (iv) manual tracing around the total area of the tissue; (v) thresholded image of total tissue area; (vi) outlined cartoon image of total area corresponding to a single count and area measurement. Scale bar represents 200 µm.

Table 2. ImageJ output showing count and area measurements following thesholding. Each count corresponds to an area in the outlined cartoon image. To determine whether the detected particle was an adipocyte cell, the outline image was assessed visually by comparing it to its corresponding MT stained image.

Area per adipocyte			Area of adipose tissue	
Count	Area (µm^2)	Adipocyte (Y/N)	Count	Area (µm^2)
1	41607.0	Y	1	948703.312
2	112557.5	Y		
3	131050.3	Y		
4	85182.3	Y		
5	268498.3	Y		
6	174925.1	Y		
7	753.0	N		

First we assessed mean adipocyte number in lymphoedema (n=9) and normal (n=7) AT samples. We compared lymphoedema leg AT to normal leg AT and found mean adipocyte number was significantly higher in AT from normal legs compared with AT from lymphoedema legs (Figure 6A, 6B, 7; $P < 0.05$). We then compared lymphoedema arm AT to normal arm AT and found mean adipocyte number was not significantly different in AT from lymphoedema arms compared with AT from normal arms (Figure 5A, 5B, 7; $P > 0.05$). Next we assessed mean adipocyte size in lymphoedema (n=9) and normal (n=7) AT samples. We found no significant difference in mean adipocyte size in AT from lymphoedema arms or legs compared with AT from normal arms or legs (Figure 5A, 5B, 6A, 6B, 8; $P > 0.05$). Therefore, adipocyte cell number is higher in normal leg AT compared with lymphoedema leg AT, but is similar in lymphoedema and normal arm AT (Figure 7). Adipocyte cell size appears to be similar in lymphoedema and normal AT (Figure 8).

The proportion of non-adipocyte cells in lymphoedema and normal AT was also assessed to determine whether this observation was more widespread in lymphoedema AT. To calculate the proportion of non-adipocyte cells, the sum of the area per adipocyte was subtracted from the total area of the tissue (Table 2). Because some AT samples contained areas with collagen and blood vessels, area measurements for collagen and blood vessels were made by thresholding the image and converting it to an outlined cartoon image to get area measurements. These measurements were then also subtracted from the total area of the tissue (Table 2). We found no significance difference in the proportion of non-adipocyte cells/mm^2 in AT from lymphoedema arms or legs compared with AT from normal arms or legs (Figure 9; $P > 0.05$).

6.4 Collagen content is similar in lymphoedema and normal AT

Since AT can contain collagen, and MT and PSR staining of lymphoedema AT revealed areas with collagen deposition (Figure 3A(iv,v), 3B(iv,v)), we examined AT from lymphoedema patients to estimate the extent (if any) of collagen present and compared it to normal AT. Using ImageJ processing software, we developed a microscopic image analysis method to estimate the proportion of collagen content (Figure 10). In order to achieve a representative assessment of collagen content in AT samples (since collagen content was otherwise dependent on the field of view taken), MT stained light microscopy images of the entire tissue section (n=16) were taken and “stitched” together using ImageJ’s stitching plugin (Figure 10(i), 11, 12). The stitched image was then separated into three fluorescent color-isolated images using ImageJ’s color deconvolution (Ruifrok and Johnston, 2001). The fluorescent color-isolated image showing only collagen areas (green or red) was then thresholded and converted to an outlined cartoon image (Figure 10(iii)), with each area numbered to give corresponding area measurements (Table 3). To calculate proportion of collagen content per area of the AT sample, an outline was manually traced around the total area of the tissue (Figure 10(iv)). A ‘mask’ of this trace was then created to allow the image to be thresholded (Figure 10(v)) and converted into an outlined cartoon image (Figure 10(vi)) to give a single area measurement (Table 3). We then assessed collagen content in lymphoedema (n=9) and normal (n=7) AT samples. We found no significant difference in the proportion of collagen content/mm^2 in AT from lymphedema arms or legs compared with AT from normal arms or legs (Figure 13; $P > 0.05$).

Lymphoedema arm adipose tissue

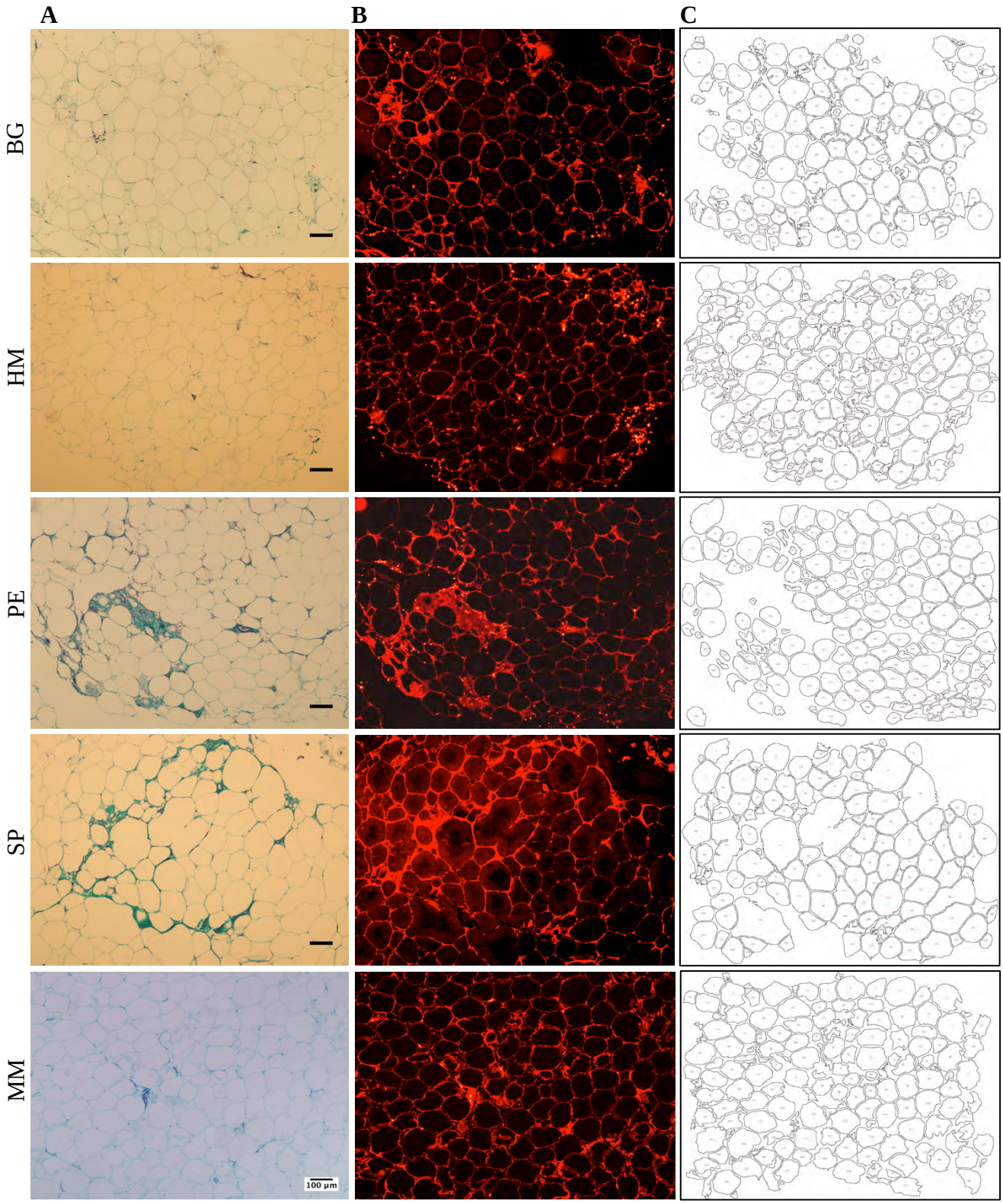

Normal arm adipose tissue

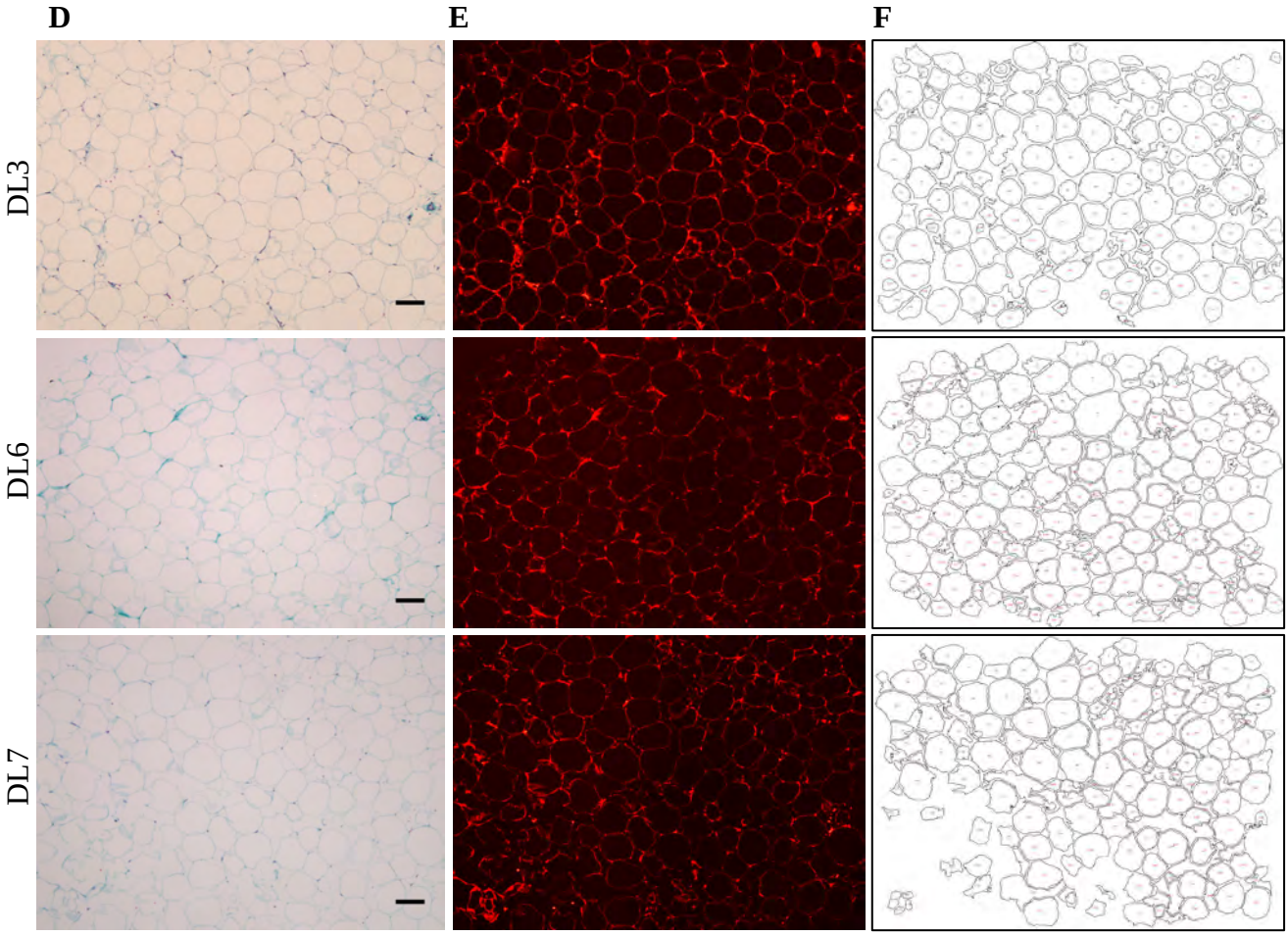

Figure 5. Lymphoedema and normal arm AT samples used to quantify adipocyte cell number and size at 10X magnification. MT stained light microscopy image of AT from **(A)** lymphoedema arm and **(D)** normal arm. Corresponding epifluorescent image of AT from **(B)** lymphoedema arm and **(E)** normal arm. Outlined cartoon image obtained following thresholding of epifluorecent image from **(C)** lymphoedema arm AT and **(F)** normal arm AT. Initials to the left of the figure represent the initials of a primary lymphoedema arm patient (MM), secondary lymphoedema arm patients (BG, HM, PE, SP) and the order we received AT samples from Dr. Lanzer's clinic (DL3, DL6, DL7). Scale bars represent 100 µm.

Lymphoedema leg adipose tissue

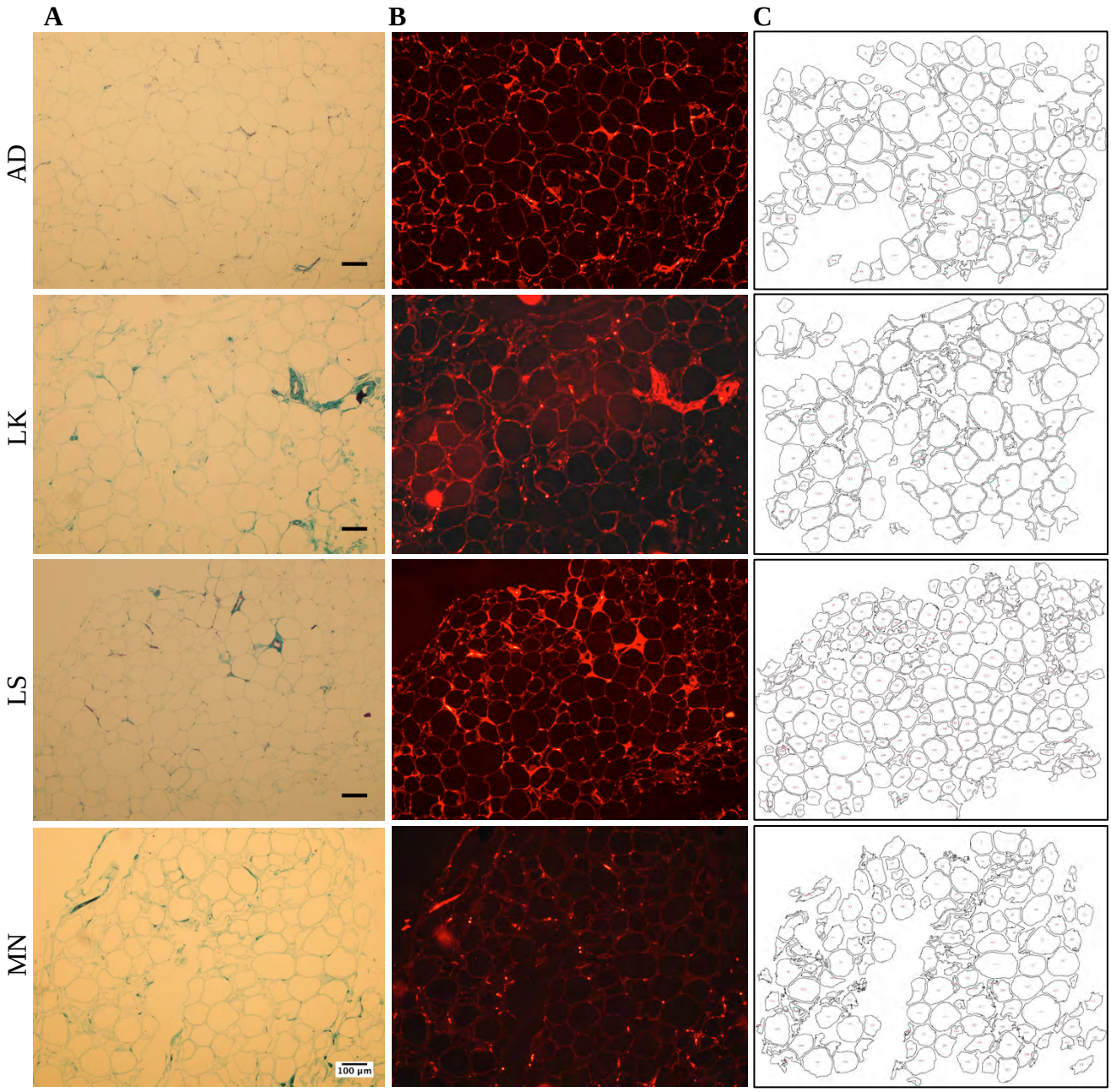

Normal leg adipose tissue

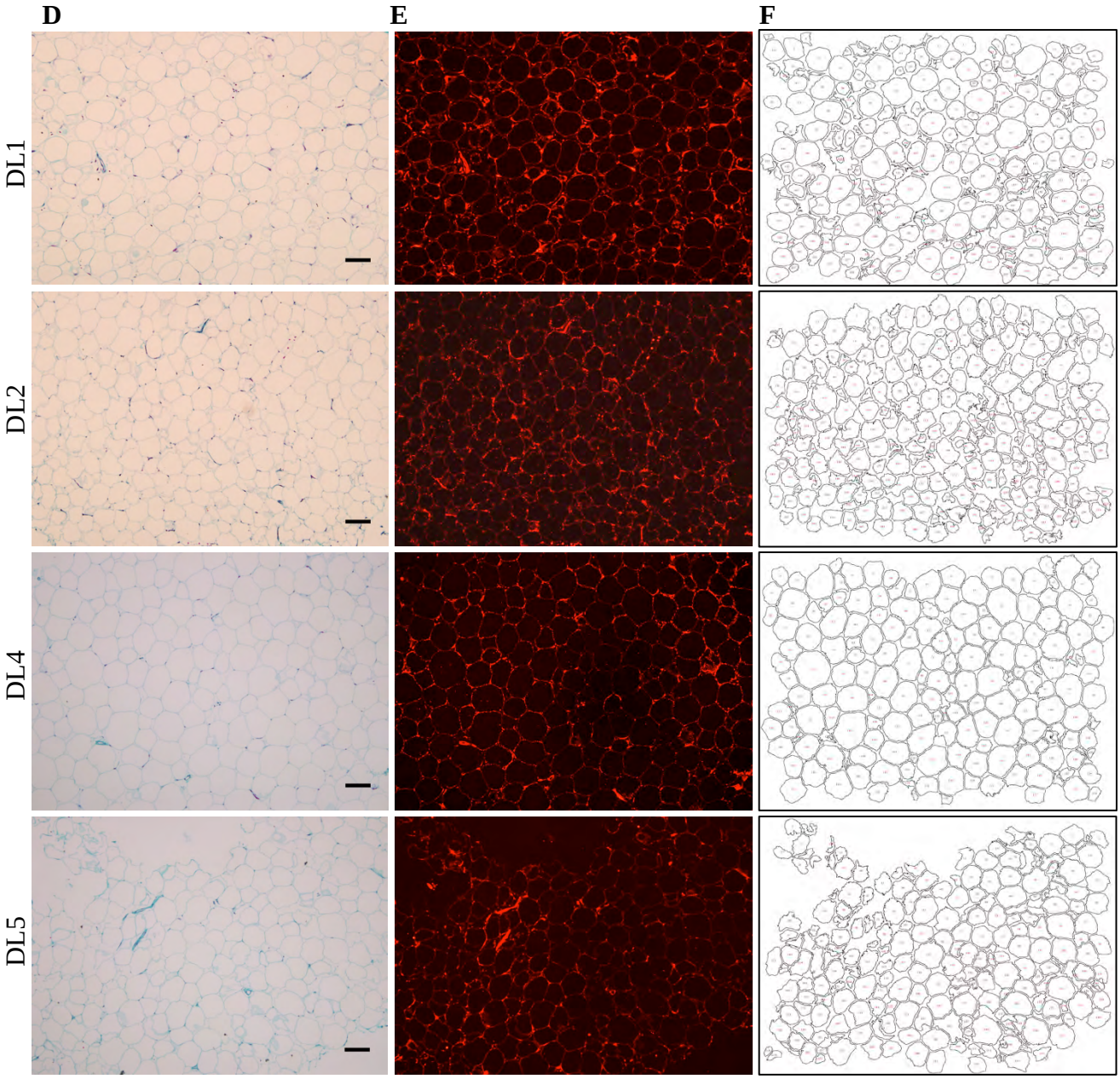

Figure 6. Lymphoedema and normal leg AT samples used to quantify adipocyte cell number and size at 10X magnification. MT stained light microscopy image of AT from **(A)** lymphoedema leg and **(D)** normal leg. Corresponding epifluorescent image of AT from **(B)** lymphoedema leg and **(E)** normal leg. Outlined cartoon image obtained following thresholding of epifluorecent image from **(C)** lymphoedema leg AT and **(F)** normal leg AT. Initials to the left of the figure represent the initials of lymphoedema leg patients (AD, LK, LS, MN) and the order we received leg AT samples from Dr. Lanzer's clinic (DL1, DL2, DL4, DL5). Scale bars represent 100 µm.

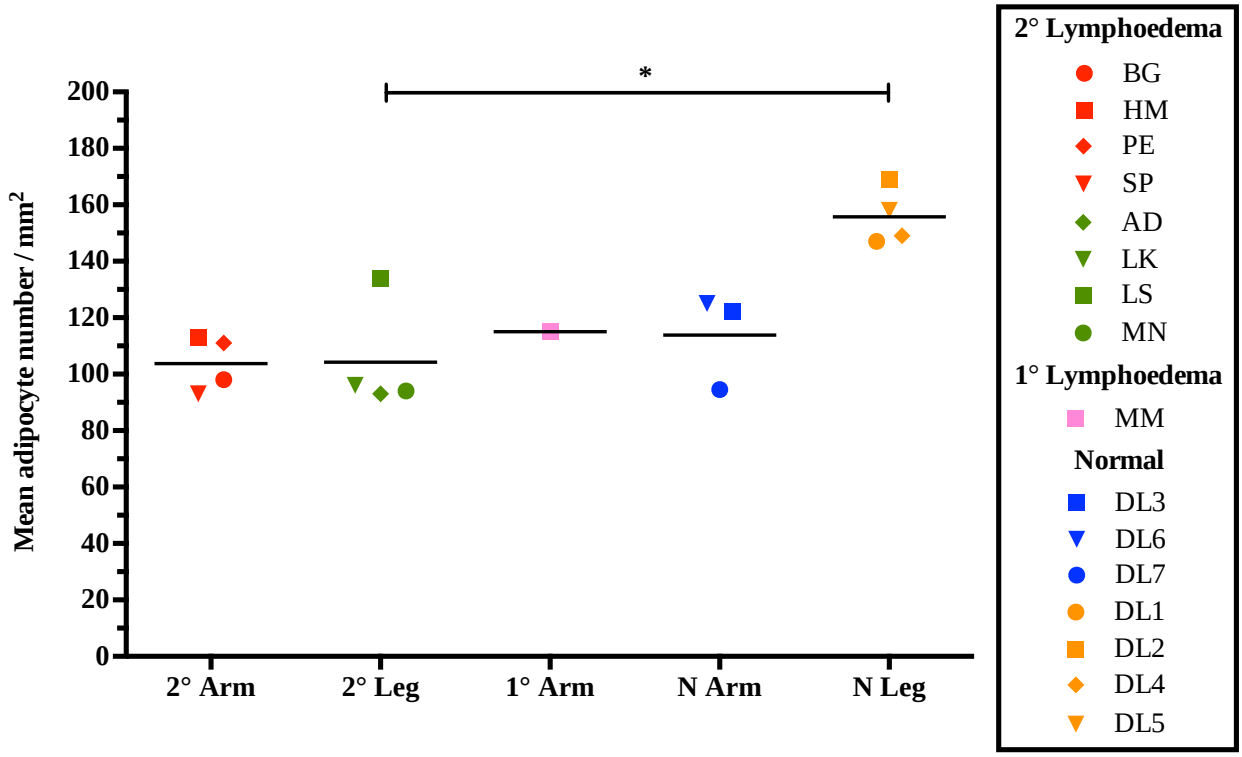

Figure 7. Mean adipocyte number / mm^2 in liposuction-derived AT samples from a primary (1°) lymphoedema arm, secondary (2°) lymphoedema arms and legs, and normal arms and legs. *$P < 0.05$.

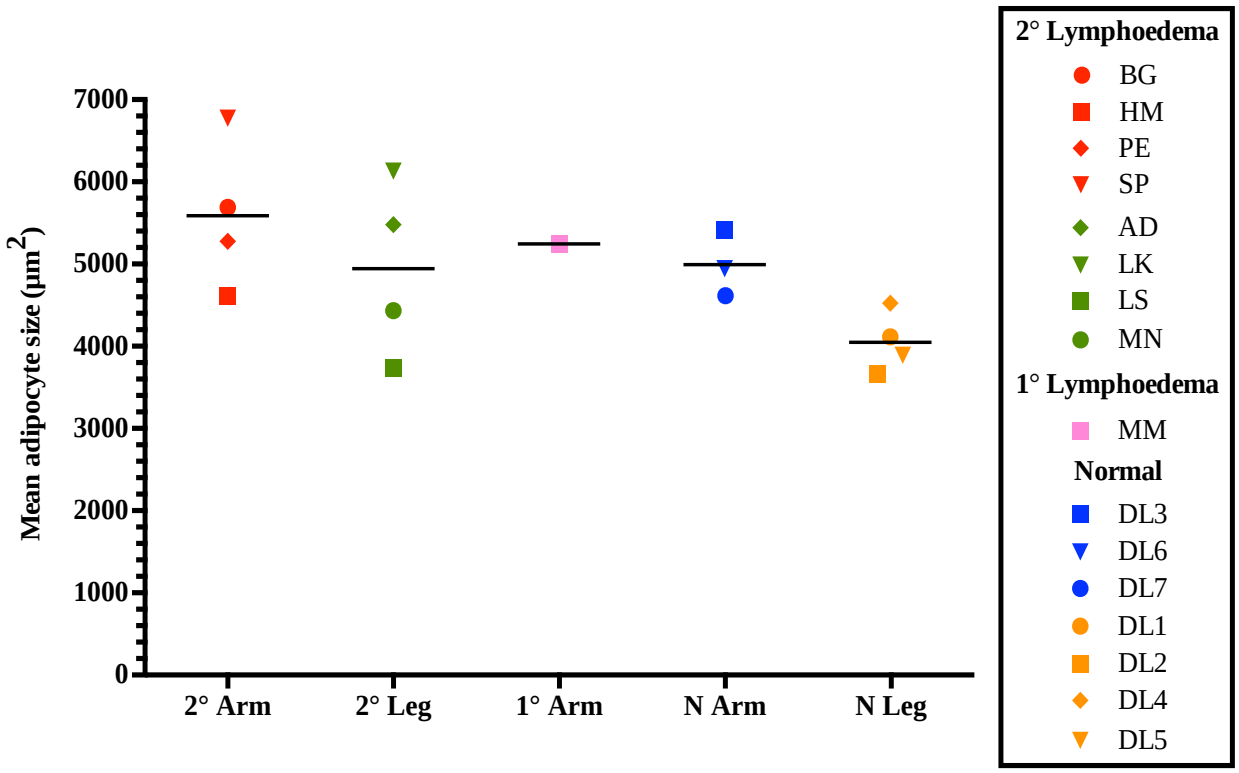

Figure 8. Mean adipocyte size (µm ^{2}) in liposuction-derived AT samples from primary (1°) arm lymphoedema, secondary (2°) arm and leg lymphoedema, normal arm and normal leg.

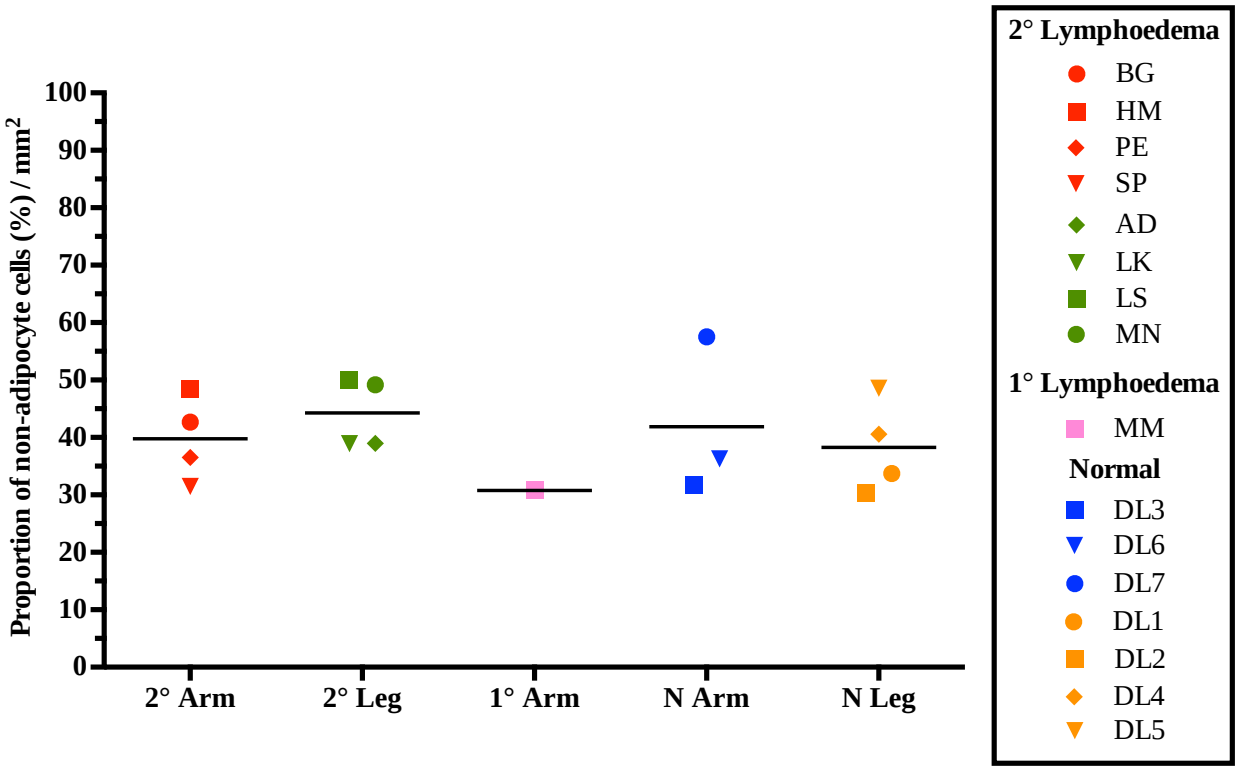

Figure 9. Proportion of non-adipocyte cells (%) / mm^2 in liposuction-derived AT samples from a primary (1°) lymphoedema arm, secondary (2°) lymphoedema arms and legs, and normal arms and legs.

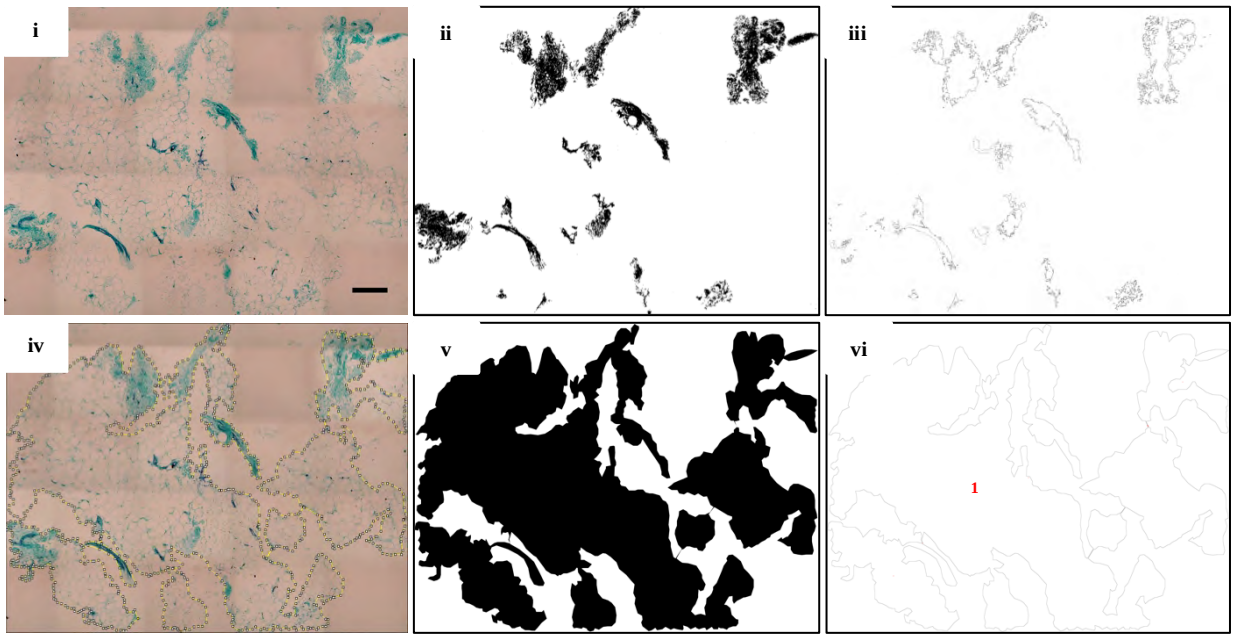

Figure 10. Image analysis method used to quantify collagen content. (i) Stitched MT stained AT viewed under light microscopy at 10X magnification; (ii) thresholded image of stitched MT stained image; (iii) outlined cartoon image showing numbered collagen areas that correspond to count and area measurements; (iv) manual tracing around the total area of the tissue; (v) thresholded image of total tissue area; (vi) outlined cartoon image of total area corresponding to a single count and area measurement. Scale bar represents 500 µm.

Table 3. ImageJ output analysis of collagen fibers in Figure 10 showing count and area measurements following thresholding. Each count corresponds to an area in the outlined cartoon image.

Area per collagen fiber		**Total area of adipose tissue**	
Count	Area (µm^2)	Count	Area (µm^2)
1	4483.5	1	11280279
2	280371.7		
3	11623.3		
4	4373.2		
5	89273.21		
6	1745.1		
7	250743.4		
…	…		
27	24424.2		

A Lymphoedema arm adipose tissue

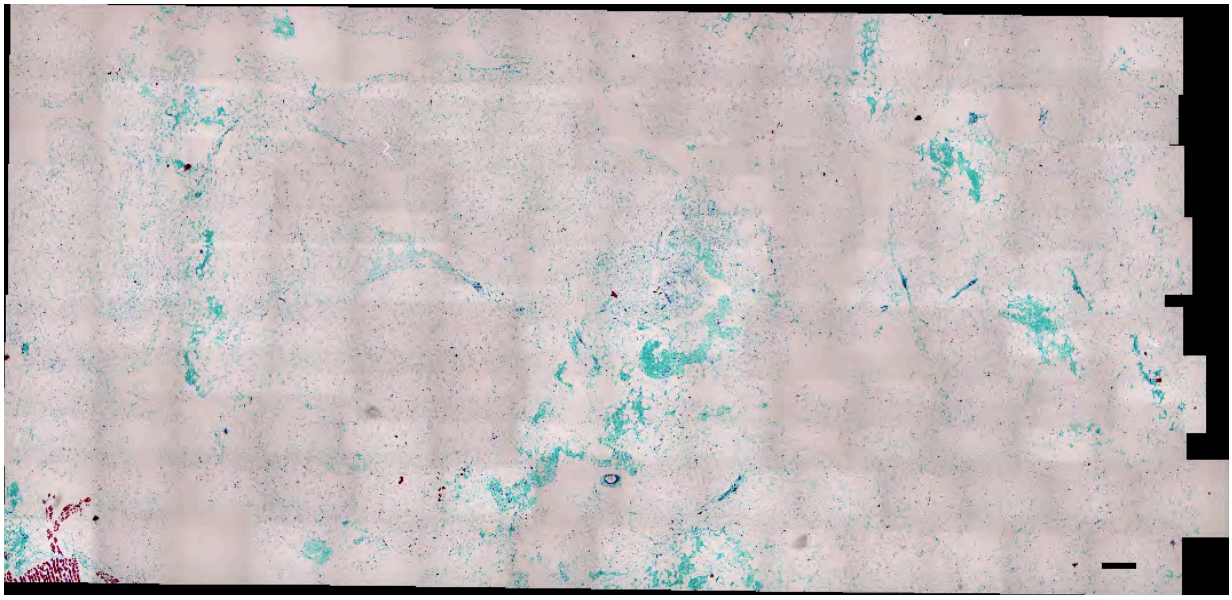

B Normal arm adipose tissue

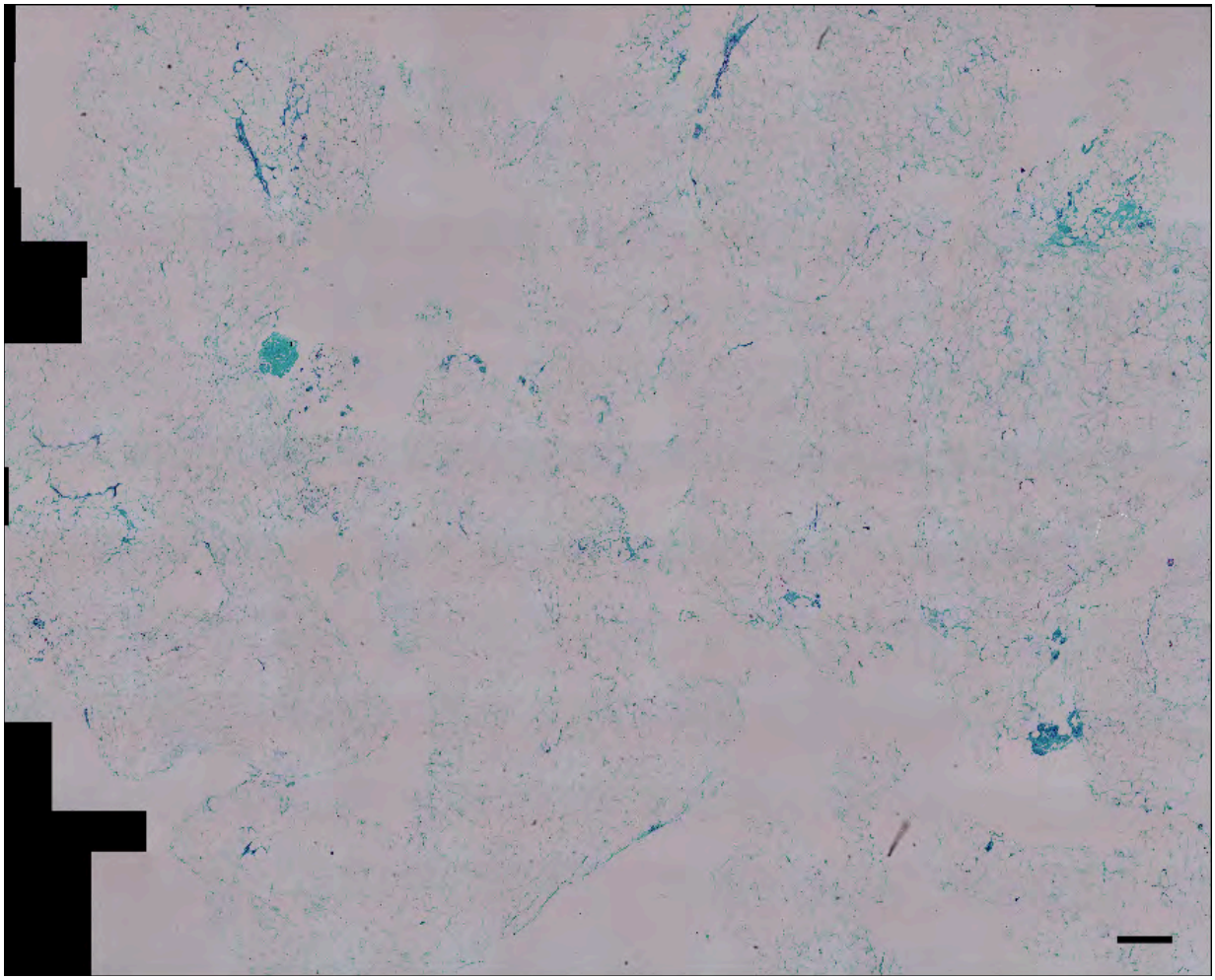

Figure 11. Stitched image of AT from **(A)** lymphoedema arm, patient HM and; **(B)** normal arm, patient DL3 at 10X magnification. Scale bars represent 500 µm.

A Lymphoedema leg adipose tissue

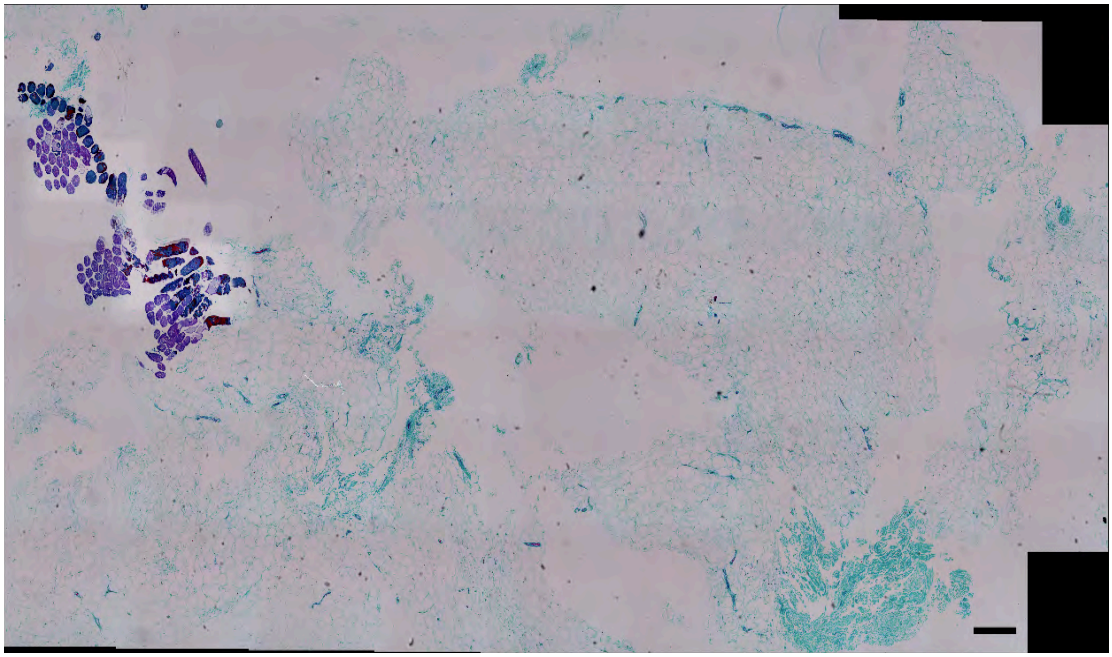

B Normal leg adipose tissue

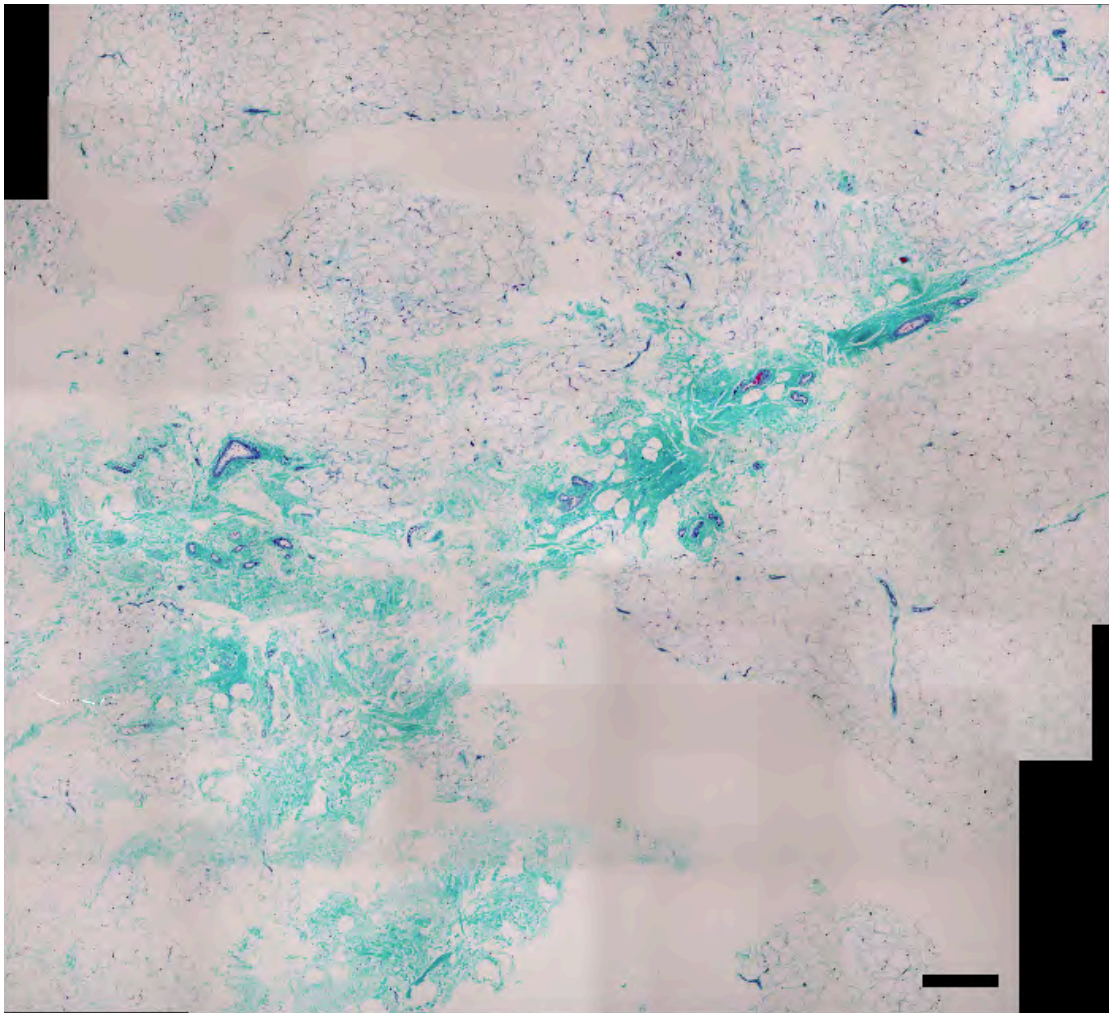

Figure 12. Stitched image of AT from **(A)** lymphoedema leg, patient MN and; **(B)** normal leg, patient DL1 at 10X magnification. Scale bars represent 400 µm.

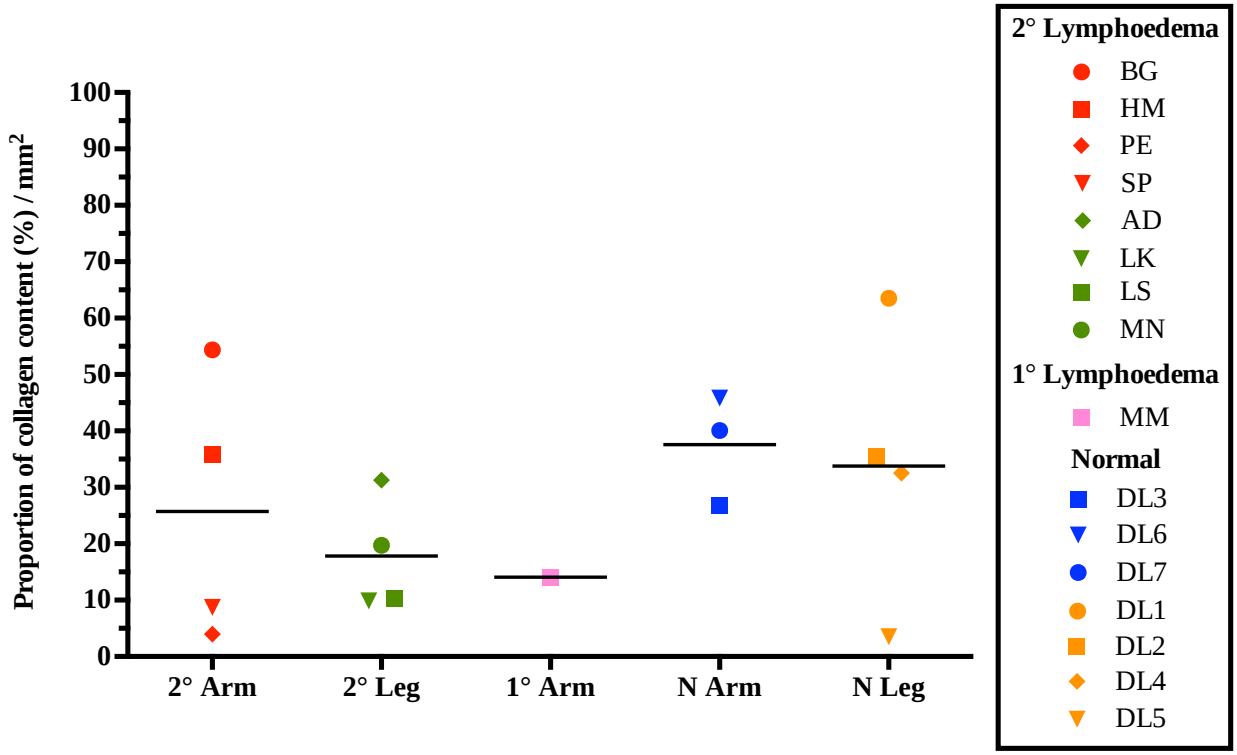

Figure 13. Proportion of collagen content (%) / mm^2 in liposuction-derived AT samples from a primary (1°) lymphoedema arm, secondary (2°) lymphoedema arms and legs, and normal arms and legs.

6.5 IHC detection of macrophages in lymphoedema AT

To determine whether the leukocytes present in lymphoedema AT are macrophages (Mφ), immunohistochemistry (IHC) was performed on AT samples from lymphoedema patients using Mφ-specific surface markers, HAM56, CD40 (M1-type Mφ), and CD206 (M2-type Mφ). Moreover, given the abundance of Mφ-like cells in lymphoedema AT, it is possible that fibrosis in lymphoedema involves Mφ-derived transforming growth factor β (TGFβ), thus a antibody specific for TGFβ was also used.

We needed to establish the method for IHC first using HAM56, CD206, and TGFβ antibodies, which have been previously described (Aron-Wisnewsky et al., 2009; Divoux et al., 2010). Sections were incubated with anti-HAM56, anti-CD206 (R&D Systems, Minneapolis, USA), anti-TGFβ (R&D Systems) specific antibodies or with no primary antibody, and detected with a goat anti-mouse IgG or a goat anti-mouse IgM HRP conjugate (In Vitro technologies, Mount Wellington, NZ). For a positive control, liver tissue was used. However, no positive staining for HAM56, CD206 or TGFβ was detected in either the lymphoedema AT sections or control liver tissue (Figure 14). Therefore, optimization of IHC methods was needed.

6.6 Optimization of IHC methods using different antigen retrieval methods

For IHC optimization, first different antigen retrieval methods were trialed. Initially, antigen retrieval was performed by microwave heating the sections in a citrate buffer solution (pH 6.0) prior to immunostaining. However, no target staining was detected (Figure 14). To determine whether the lack of target staining was due to the antigen retrieval solution used, optimization tests were conducted to compare lymphoedema AT sections treated with citrate buffer (pH 6.0), tris/EDTA buffer (pH 9.0) or no antigen retrieval. Spleen tissue was used as a positive control and sections were incubated with anti-HAM56, anti-CD40 (R&D Systems) specific antibodies or with isotype IgM or isotype IgG controls. In all cases there was no positive staining detected, either in the lymphoedema AT or spleen tissue (Figure 15). A similar result was also observed when the primary antibody concentrations was increased from a 1:100 dilution to a 1:50 dilution (data not shown).

Since no positive IHC staining was detected, even after a change in antigen retrieval treatment solution, the viability of the secondary antibodies was assessed using an avidin-biotin detection system (DAKO, Glostrup, Denmark) against our HRP conjugated detection system (R&D Systems). A spleen tissue sample was incubated with anti-CD40 specific antibody or with isotype IgG control, and detected with a biotinylated goat anti-mouse IgG secondary antibody (DAKO) or our goat anti-mouse IgG HRP conjugated secondary antibody (R&D Systems). Again, no positive staining was detected in the spleen tissue and no obvious difference was observed between the HRP conjugated secondary antibody and the biotinylated secondary antibody (Figure 16).

6.7 Optimization of IHC using DAKO reagents

Because no positive IHC target staining was detected in all previous attempts, an external test of DAKO reagents was conducted at the Kolling Institute of Medical Research (St Leonards, New South Wales) by Mr. Rowan Ikin, using antibodies specific for blood endothelial cells (BEC) (CD31), smooth muscle actin (SMA), and vimentin. For this, IHC staining was examined on human liver, colon and appendix tissues, as well as lymphoedema AT. Sections were incubated with the specific primary antibody or with isotype IgG control, and detected with a EnVisionTM FLEX polymer-HRP secondary antibody (DAKO). Positive staining for SMA, and vimentin was detected in the liver tissue; CD31 positive and vimentin positive

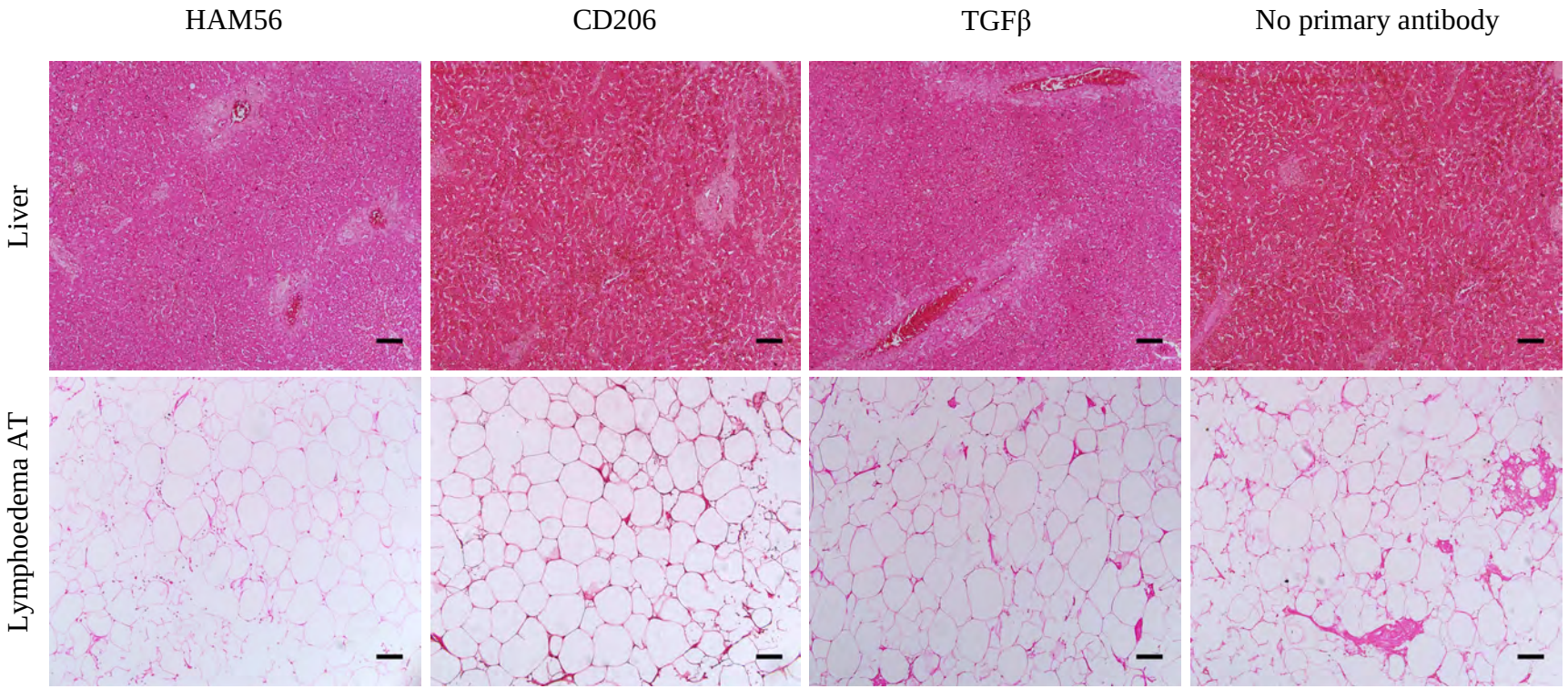

Figure 14. IHC detection of macrophages in lymphoedema AT. Lymphoedema AT and liver sections were incubated with HAM56, CD206, TGFβ or no primary antibody diluted at 1:100, and detected with IgG- or IgM-HRP conjugated secondary antibody. Images are representative of two different lymphoedema patients at 10X magnification. Scale bars represent 100 μm.

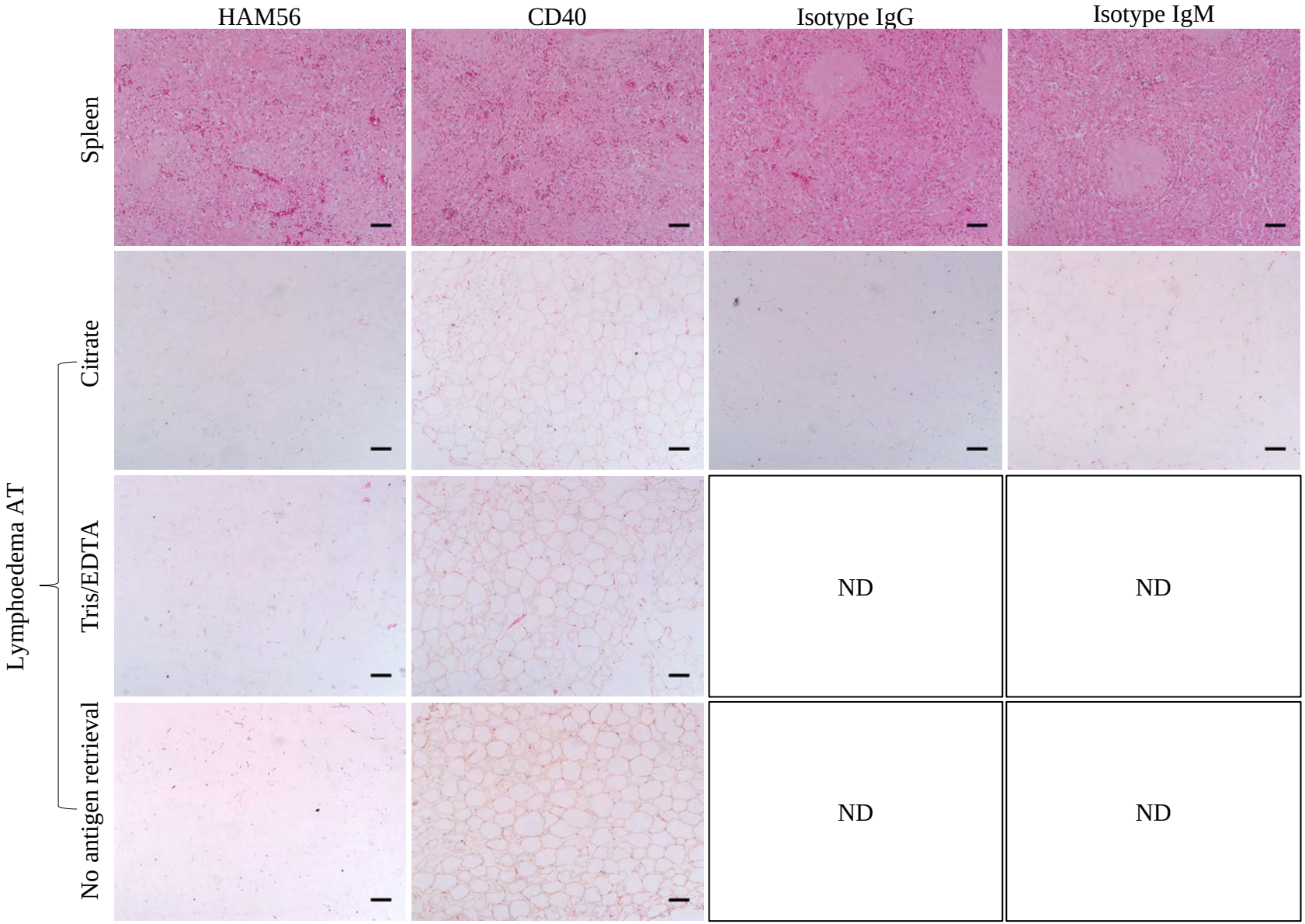

Figure 15. Optimization of IHC using different antigen retrieval methods. Lymphoedema AT and spleen sections were treated with citrate buffer (pH 6.0), Tris/EDTA buffer (pH 9.0) or no antigen retrieval. Sections were incubated with HAM56, CD40 or IgG/IgM isotype controls diluted at 1:100, and detected with IgG- or IgM-HRP conjugated secondary antibody. Images are representative of three different lymphoedema patients at 10X magnification. ND: not done. Scale bars represent 100 μm.

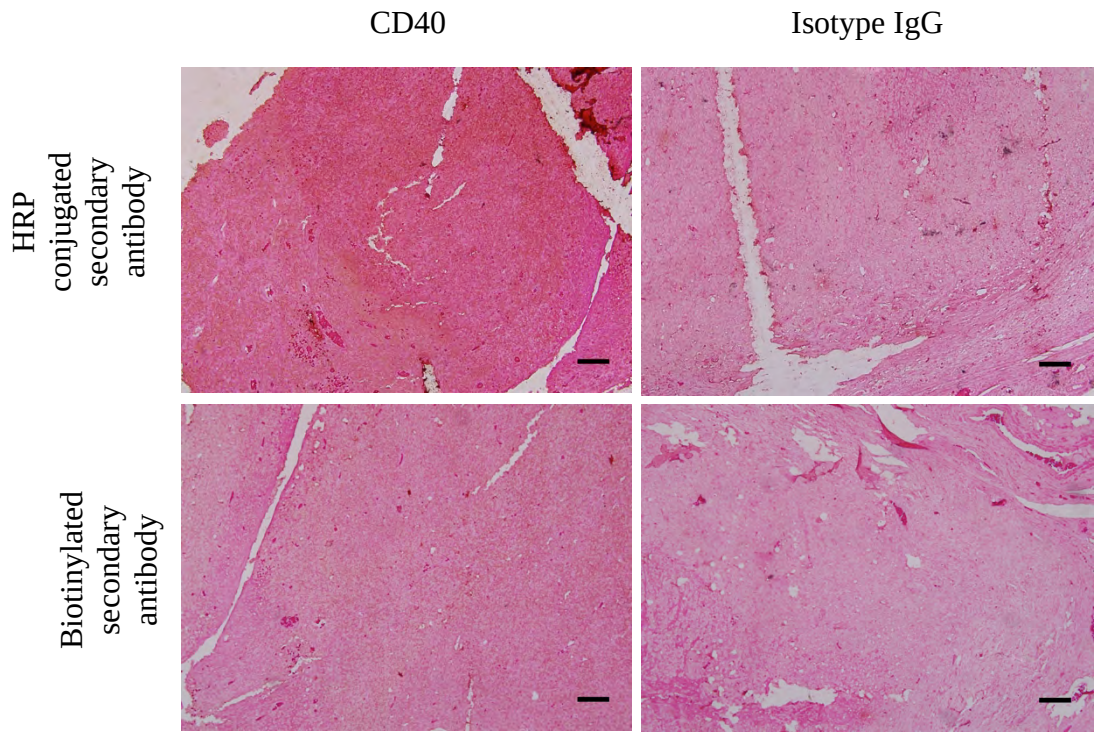

Figure 16. Optimization test on the viability of the HRP conjugated detection system (R&D Systems). Spleen sections were incubated with CD40 primary antibody or IgG isotype control diluted at 1:100, and detected with HRP conjugated secondary antibody (R&D Systems) or biotinylated secondary antibody (DAKO). 10X magnification. Scale bars represent 100 µm.

cells was detected in the colon; and SMA positive and vimentin positive cells was detected in the appendix (Figure 17). Positive staining for CD31, SMA, and vimentin was also detected in lymphoedema AT, and as expected, no isotype IgG staining was detected (Figure 17). Thus, it appeared that the DAKO EnVisionTM amplified system and DAKO reagents, such as wash buffers, were required to perform IHC on formalin-fixed paraffin-embedded AT.

A second validation test was conducted on lymphoedema AT and AT from healthy individuals. Sections were incubated with anti-CD31, anti-podoplanin, anti-SMA specific antibodies or with isotype IgG control, and detected with a EnVisionTM FLEX polymer-HRP secondary antibody. For a positive control, liver tissue was included in the experiment. Positive staining for CD31, podoplanin, and SMA was detected in lymphoedema AT and in normal AT (Figure 18). As expected, no isotype IgG staining was detected, but there was clear CD31 positive, podoplanin positive, and SMA positive staining in the liver tissue (Figure 18). Therefore, using DAKO reagents we established an IHC method for detecting lymphatic endothelial cells (LEC) and blood vascular endothelial cells (BEC) in liposuction-derived AT.

6.8 Optimization of counterstains for IHC detection of SMA in lymphoedema AT

To improve visualization of IHC stained cells, and assessment of tissue morphology, AT sections were incubated with CD31 and podoplanin specific antibodies, and detected with a EnVisionTM FLEX polymer-HRP secondary antibody. Sections were then counterstained with a fast green and hematoxylin (alcoholic eosin with phloxine counterstain was not used as it was not a good contrast color with brown DAB positive cells (Figure 14-16). Five counterstain conditions were tested - fast green alone, hematoxylin alone, application of fast green followed by hematoxylin, application of hematoxylin followed by fast green, or no counterstain. Sections were incubated with anti-SMA specific antibody, since we established positive staining for SMA in lymphoedema and normal AT (Figure 17-18). For a positive control, liver tissue was used; but no negative isotype IgG control was used, since we simply wanted to optimize the counterstaining step of the IHC procedure. Hematoxylin alone and fast green alone counterstains produced a high level of contrast between the brown DAB positive cells in the liver tissue (Figure 19). However, in subsequent fast green counterstaining, the fast green was diluted in glacial acetic acid, and the time in which the fast green was left on the tissue was reduced from one min to 15 sec. In lymphoedema AT, hematoxylin produced a high level of contrast between the brown DAB positive cells, however hematoxylin only stained cell nuclei and it did not act as a good counterstain, especially for the assessment of perivascular collagen (Figure 19). In contrast, there was no variability in the intensity of the fast green counterstain and staining localization of the brown DAB positive cells was easily recognized (Figure 19).

6.9 CD31 is expressed in lymphoedema and normal AT

Finally, to determine the relative location of perivascular collagen, IHC was performed on AT from lymphoedema patients (n=9) and AT from normal patients having cosmetic liposuction (n=7). Sections were incubated with anti-CD40 specific antibody or with isotype IgG control, and detected with a EnVisionTM FLEX polymer-HRP secondary antibody. For a positive control, colon tissue was used in the experiment. Lymphoedema AT from arms/legs and normal AT (arms/legs) showed positive staining for CD31, which are consistent with the endothelial cells lining blood vessels (Figure 20). As expected, no IHC staining was detected with isotype IgG control antibody (Figure 20(xi-xv)). CD31 positive IHC staining occurred in areas of collagen deposition, although some vessels that were CD31 negative were also surrounded by collagen (Figure 20(ii-v, vii-x)). However, unexpectedly no

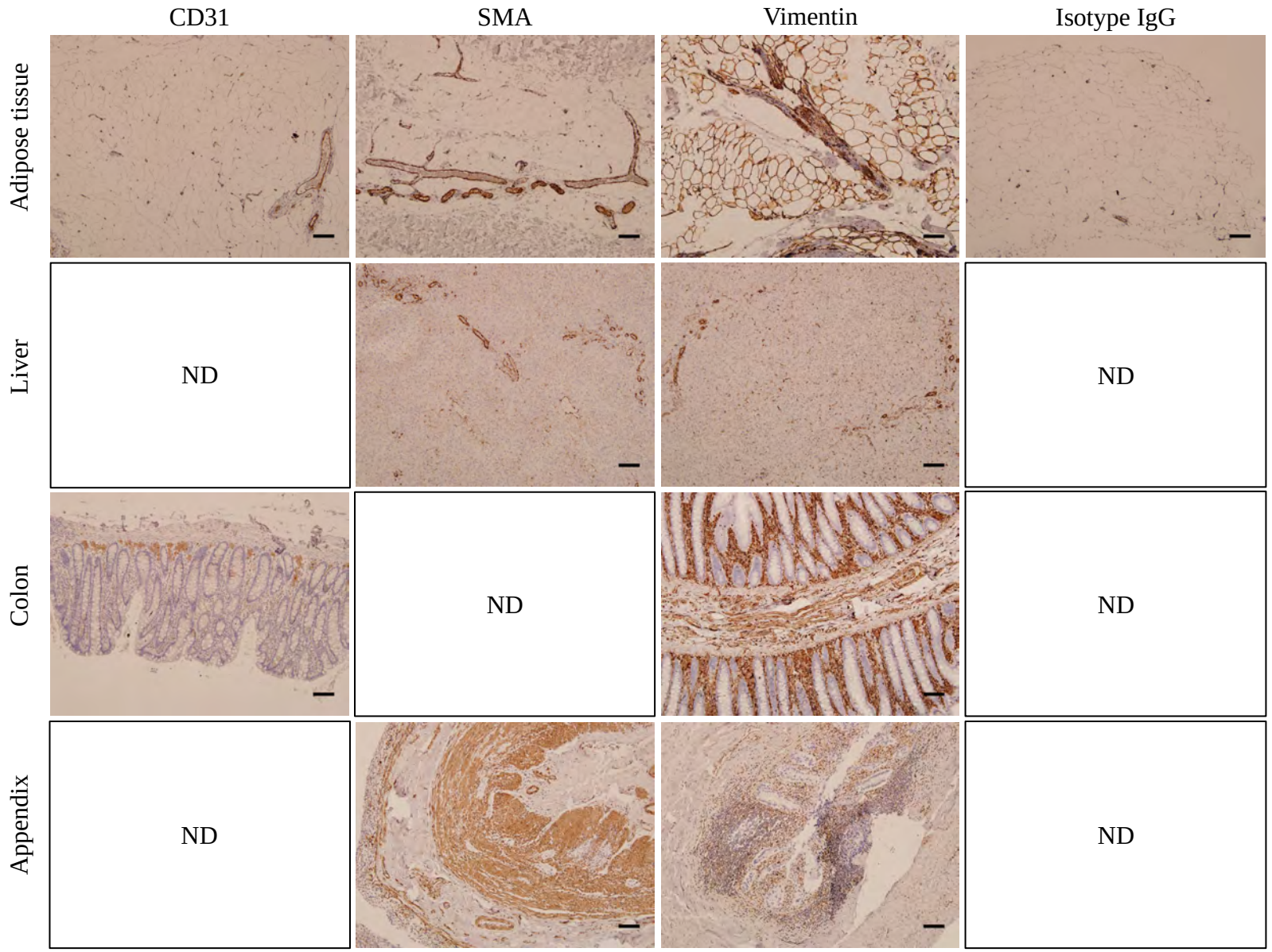

Figure 17. External test of DAKO reagents on lymphoedema AT and positive control tissues. Sections were incubated with CD31, SMA, Vimentin or IgG isotype control diluted at 1:100, and detected with DAKO EnVisionTM FLEX polymer-HRP secondary antibody. Images are representative of one lymphoedema patient at 10X magnification. ND: not done. Scale bars represent 100 µm.

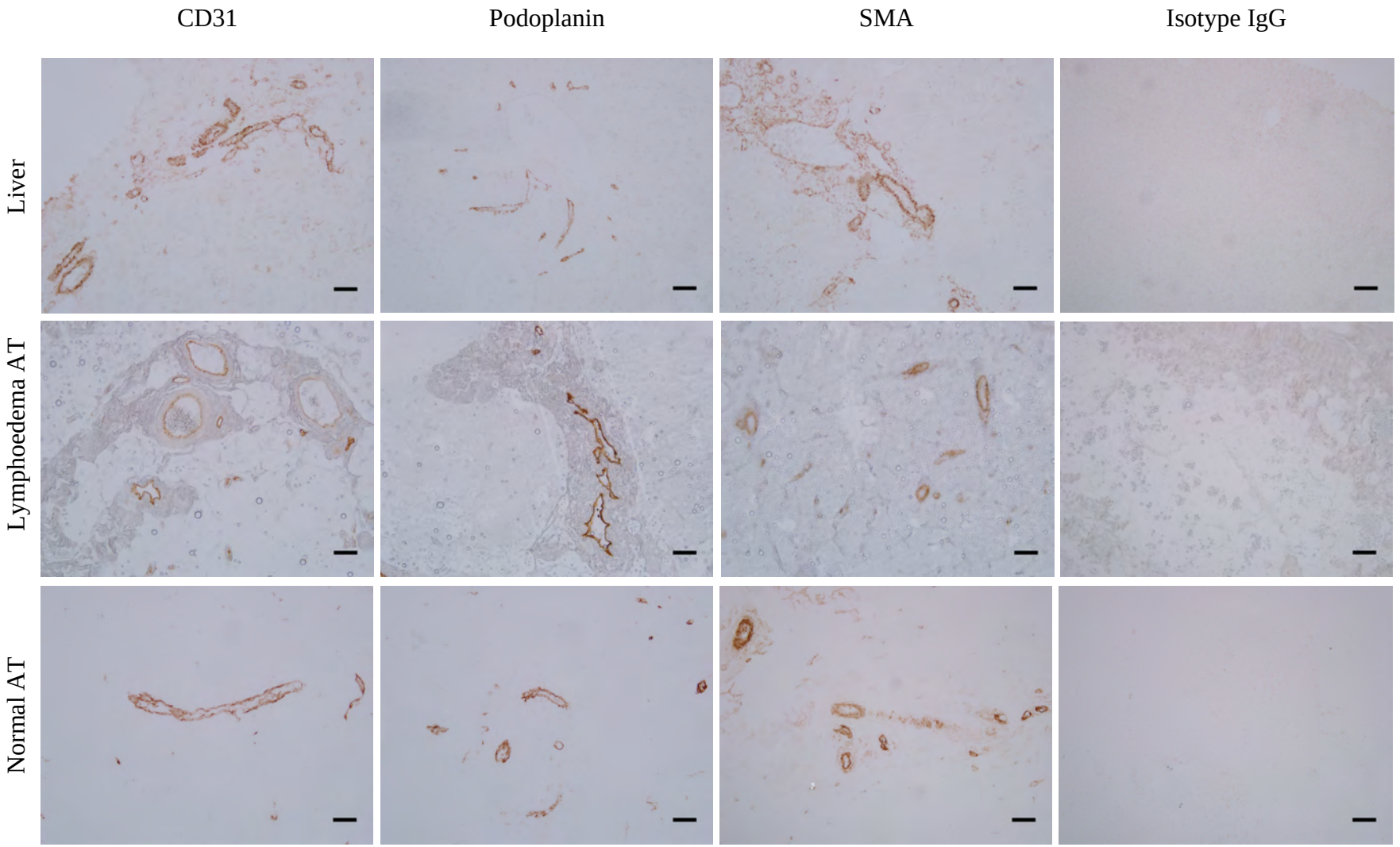

Figure 18. Validation test of DAKO reagents on lymhoedema and normal AT. Sections were incubated with CD31, Podoplanin, SMA or IgG isotype control diluted at 1:100, and detected with DAKO EnVisionTM FLEX/HRP secondary antibody. Images are representative of two lymphoedema and two normal patients at 10X magnification. Scale bars represent 100 µm.

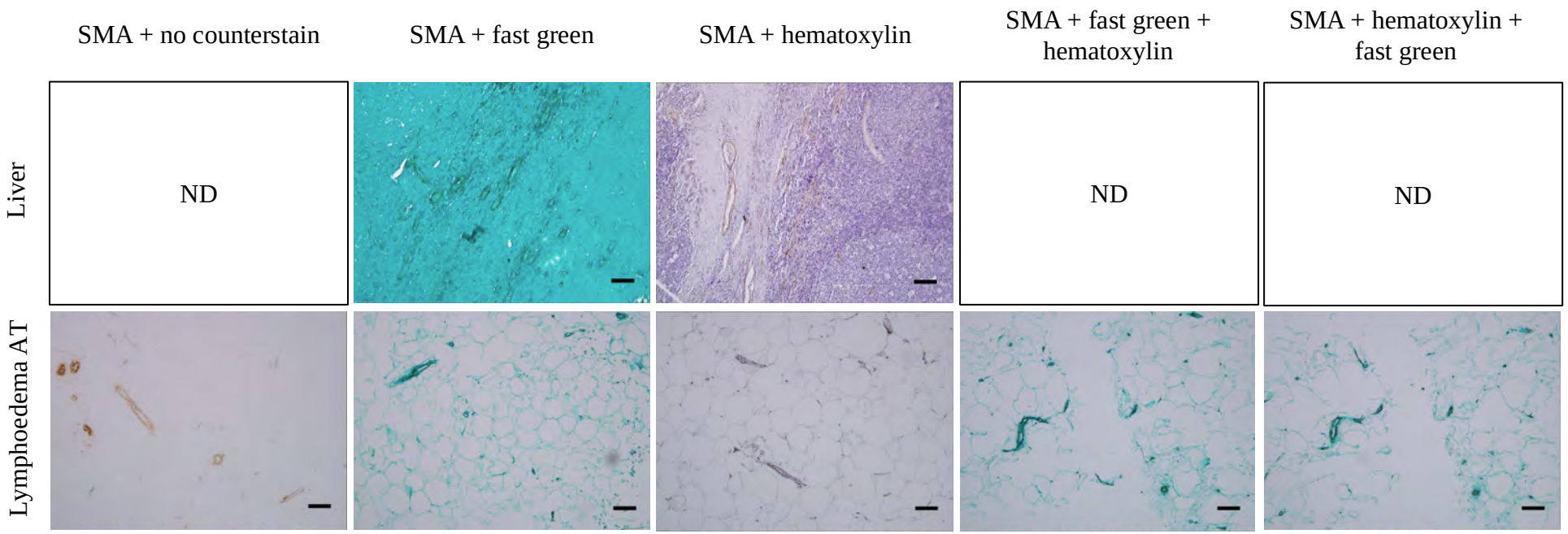

Figure 19. Optimization of counterstains for IHC detection of SMA in lymphoedema AT. A DAB only/no counterstain, fast green only, hematoxylin only, fast green + hematoxylin, hematoxylin + fast green counterstain was trialed on lymphoedema AT sections incubated with SMA at 1:100, and detected with DAKO EnVisionTM FLEX polymer-HRP secondary antibody. Images are representative of one lymphedema patient at 20X magnification. ND: not done. Scale bars represent 100 µm.

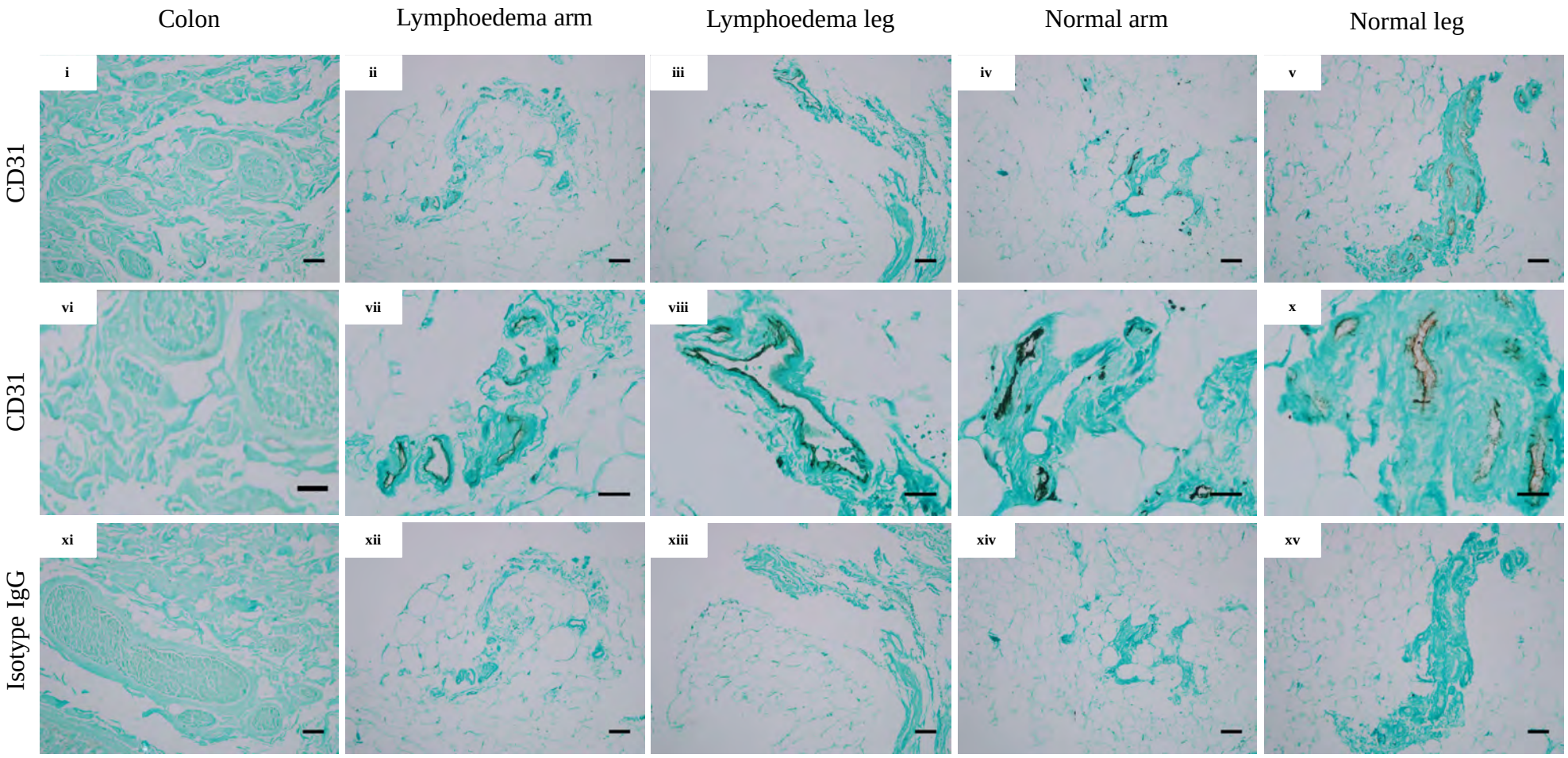

Figure 20. IHC detection of CD31 in AT from lymphoedema arm/leg and normal arm/leg. AT sections were incubated with CD31 or IgG isotype control diluted at 1:100, and detected with DAKO EnVisionTM FLEX polymer-HRP secondary antibody. CD31 dectection at (i-v) 10X magnification; (vi-x) 40X magnification. Isotype IgG detection at (xi-xv) 10X magnification. Images are representative of two lymphoedema and two normal patients. Scale bars represent 100 µm.

positive staining for CD31 was detected in the colon tissue (Figure 20(i,vi). Therefore, collagen surrounds blood vessels and possibly also lymphatic vessels.

To confirm this interpretation and to determine if lymphatic vessels are similarly surrounded by collagen, IHC was performed with an antibody specific to podoplanin, which is specific for lymphatic endothelial cells (LEC) (Schacht et al., 2003), and is not expressed on BEC. Lymphoedema (n=9) and normal (n=7) AT were incubated with anti-podoplanin antibody or with isotype IgG control, and detected with a EnVisionTM FLEX polymer-HRP secondary antibody. For a positive control, liver tissue was used in the experiment. Unfortunately, no podoplanin positive vessels were evident (Figure 21), and this was also found when sections were incubated with anti-podoplanin antibody at an increased concentration (diluted at 1:50) (Figure 22A) and diluted at 1:50 and incubated overnight at 4℃ (Figure 21B). Therefore, further optimization of IHC methods are needed to be able to detect podoplanin positive expression on formalin-fixed AT sections. Nevertheless, it is likely that the CD31 negative vessels that are surrounded by collagen are lymphatic vessels, given that there are only two types of vessels – blood or lymph vessels.

6.10 HAM56 expression is not evident in lymphoedema AT

To determine whether Mφ are present in lymphoedema AT, and hence confirm histological observations that indicate the presence of abundant Mφ-like leukocyte cells, IHC was performed on lymphoedema and normal AT samples using a Mφ-specific surface antigen, HAM56. For controls, a liver tissue positive control and a isotype IgM control was used. Unfortunately, no positive staining for HAM56 was detected in either lymphoedema AT or normal AT or liver tissue (Figure 23). Therefore, further optimization tests are also needed to determine the identity of the macrophage-like cells in lymphoedema AT.

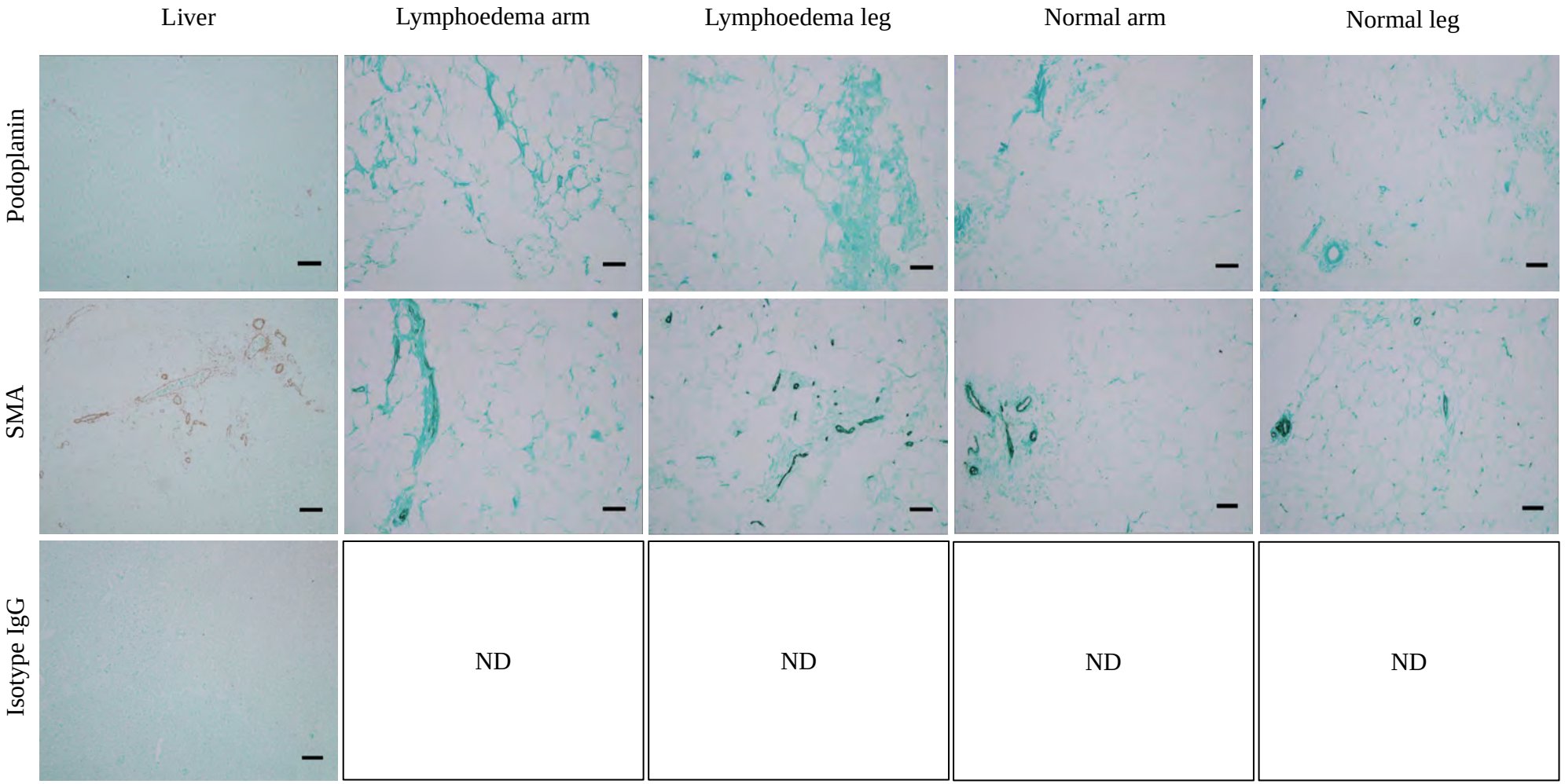

Figure 21. IHC detection of Podoplanin in AT from lymphoedema arm/leg and normal arm/leg. AT sections were incubated with Podoplanin or IgG isotype control diluted at 1:100, and detected with DAKO EnVisionTM FLEX polymer-HRP secondary antibody. Images are representative of two lymphoedema and two normal patients at 20X magnification. ND: not done. Scale bars represent 100 µm.

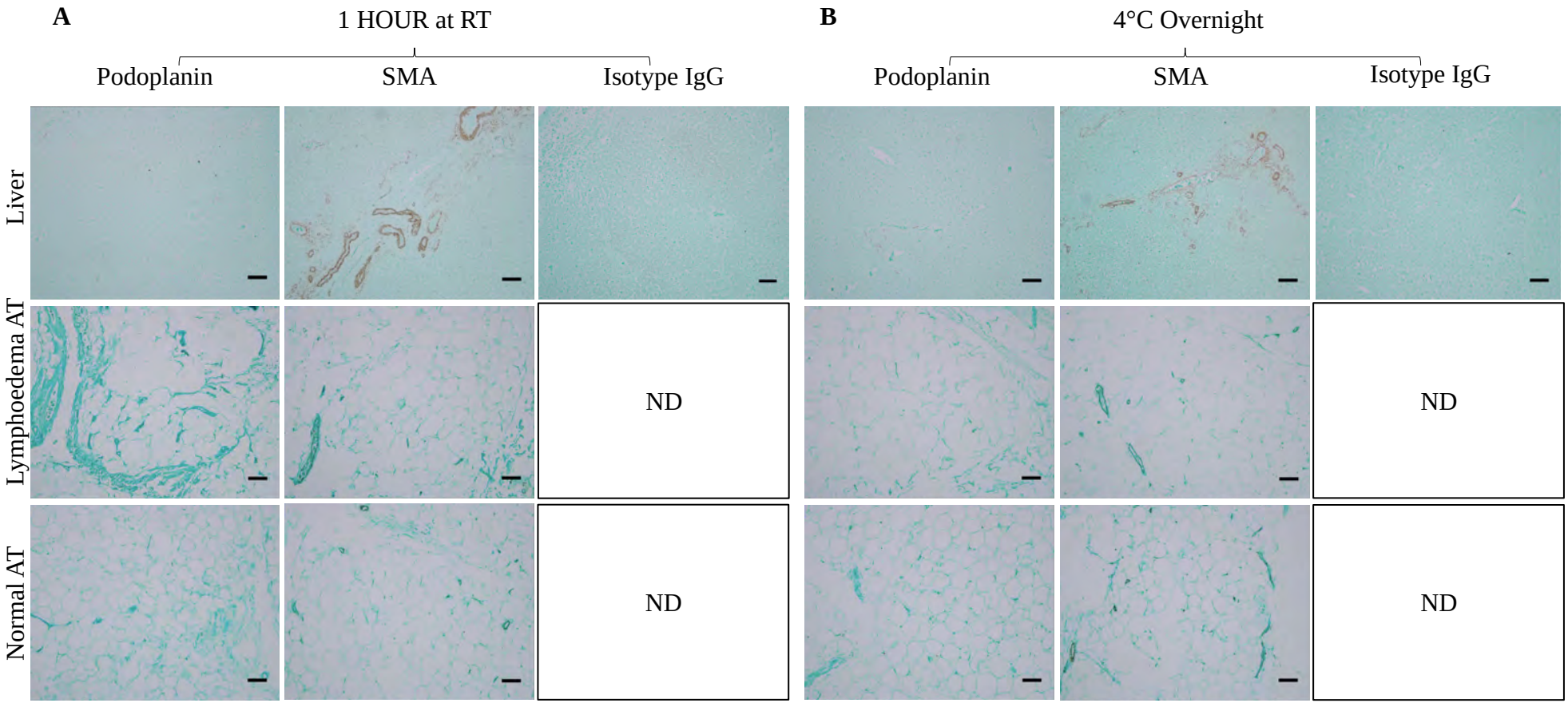

Figure 22. IHC detection of Podoplanin in lymphoedema and normal AT. AT sections were incubated with Podoplanin or IgG isotype control diluted at **(A)** 1:100 and **(B)** 1:50 and incubated overnight at 4°C. Images are representative of one lymphoedema and one normal patient at 20X magnification. ND: not done. Scale bars represent 100 µm.

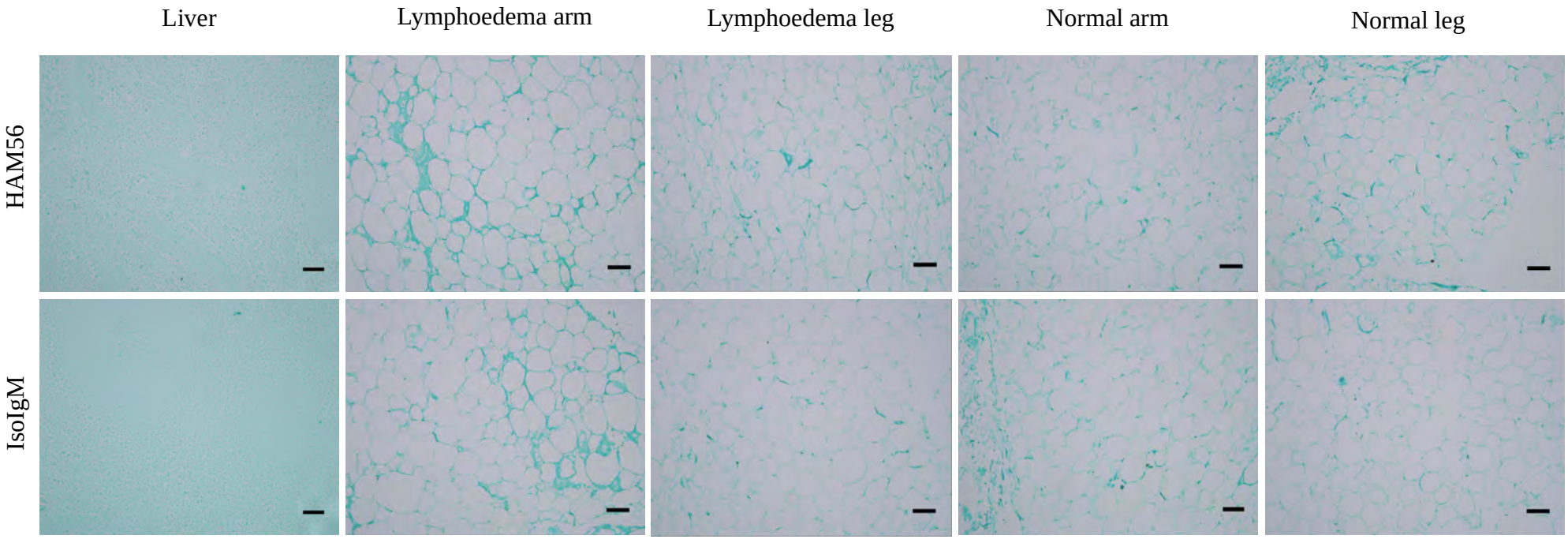

Figure 23. IHC detection of HAM56 in AT from lymphoedema arm/leg and normal arm/leg. AT and liver sections were incubated with HAM56 or IgM isotype control diluted at 1:100, and detected with IgM-HRP conjugated secondary antibody. Images are representative of two lymphoedema and two normal patients at 20X magnification. Scale bars represent 100 μm.

7. Discussion

There is minimal knowledge about the composition and pathology of adipose tissue (AT) produced in lymphoedema. Chronic interstitial fluid accumulation has been shown to incite fat deposition, fibrocyte activation and connective tissue overgrowth (Gaffney and Casley−Smith, 1981; Šmahel, 1986; Ryan, 1995). However, the extent of these pathophysiological features in human lymphedematous tissues has not been determined. The focus of this thesis was to characterize the AT removed through surgical liposuction from patients with lymphoedema, using histological analysis, image analysis, and immunohistochemistry to determine adipocyte cell number, adipocyte size, tissue fibrosity, collagen content, and the presence of macrophages (Mφ).

7.1 Random acquisition of biopsy samples

Liposuction tissue samples were obtained from lymphoedema patients' limbs (5 arms, 4 legs) and from limbs of healthy individuals undergoing cosmetic liposuction surgery (3 arms, 4 legs). Random aliquots of AT were taken directly from the liposuction bags (Figure 1) of lymphoedema and normal patients. The random acquisition of the tissue biopsy samples means that the tissue collected was not limited, nor localised to, a specific anatomical site in the affected limb. In fact, we were completely unaware of which anatomical site of the arm or leg we were sampling from. Therefore, through random biopsy sampling we obtained AT biopsy samples that are unbiased with respect to AT from lymphoedematous and normal limbs.

7.2 Uniform processing of adipose tissue

Each AT patient sample was processed under the same conditions, even though they were collected over the course of the year. All lymphoedema AT samples were processed within approximately 3-4 hr of the liposuction procedure at Macquarie University Hospital. Normal AT samples were processed within 1 hr of arrival by courier from Melbourne. However, because four normal samples (patients DL3, DL5, DL6 and DL7) required overnight courier, they were processed within 1 hr of arrival after overnight storage at 4°C, whereas samples DL1 and DL2 were transported and processed on the same day as collection. All tissue samples were fixed, embedded and processed at the Histopathology Laboratory, Department of Pathology, The University of Sydney, in the same manner. Formalin-fixed paraffin-embedded AT samples were stained with the same stains, Harris' hematoxylin and eosin (H&E), Milligan's trichrome (MT), and picrosirius red (PSR) for histological analysis using standard light microscopy. Histological analysis appeared similar in all normal liposuction AT samples, likely indicating that overnight storage at 4°C had no significant effect on the morphology of AT.

7.3 Image analysis of adipocyte cell number is a true reflection of adipose tissue

Using ImageJ processing software it was possible to develop a microscopic image analysis method to determine adipocyte cell number and size in lymphoedema and normal AT (Figure 4). Six epifluorescent images of MT stained sections were randomly acquired in the upper, middle, and bottom areas of each AT section at 10X magnification. Given the number and randomness of the images captured it is reasonable to assume that the images are representative of adipocyte cell morphology in the tissue section as a whole. This is validated in the data we obtained for adipocyte cell count where in each of the six fields of view, up to 169 adipocyte cells were counted per field. Moreover, we found similar trends in the mean adipocyte number for each patient, and an analysis of statistical normality indicated that all

sample data sets constituted a Gaussian (normal) distribution (appendix). For example, data points for mean adipocyte number in secondary lymphoedema arm/leg AT and normal arm/leg AT clustered reasonably tightly around their means (Figure 7). Therefore, adipocyte numerical data is representative of a large number of cells, and is likely a true reflection of lymphoedema and normal tissue.

7.4 Measurement of adipocyte size or lipid droplet size?

The adipocyte is unique among cells in that one component, the lipid droplet, normally encompasses greater than 95% of the entire cell body (Nishimura et al., 2007). Because the lipid droplet occupies most of the volume of the cell, the remaining 5% of its cellular mass, its cytoplasm, nucleus, and other components, are pushed towards the edges of the cell, which is bounded by a plasma membrane (Nishimura et al., 2007). It is worth noting that the area measurements taken are of the lipid droplet only. This is because in ImageJ a threshold needs to be set in order to distinguish the features of interest from its background. When a threshold is set, the image becomes segmented; and as a result, it is the area within the segmented feature that is being measured. Moreover, the thin cytoplasm of adjacent cells are indistinguishable from each other under light microscopy. Thus, the estimate of adipocyte size is really an estimate of mean lipid droplet size.

This research used conventional microscopy to determine mean adipocyte number and lipid droplet size in 2-dimensional space. Formalin-fixed paraffin-embedded AT were cut into 5 μm sections, since conventional microscopy requires viewing a thin-cut section of a fixed tissue, and cannot be used to view thick tissue samples. However, confocal microscopy could potentially be used to obtain a more accurate measurement of adipocyte size. Confocal microscopy overcomes the shortcomings of conventional microscopy by using optical imaging to create a virtual splice or plane, many micrometers deep, within the tissue. To create an image of the specimen, the desired focal point is rapidly and serially scanned in the *X*–*Y* plane (Nwaneshiudu et al., 2012). As the scanning progresses, signal from the detector is fed to a computer that collects all the “point images” of the sample and serially constructs the image one pixel at a time. Because the sample is not actually sectioned, it is possible to image a “stack” of virtual, confocal image planes that can later be used to make 3-dimensional images of tissues (Nwaneshiudu et al., 2012). Therefore, confocal microscopy analysis of thickly sliced AT might be useful to accurately reconstruct virtual 3-dimentional representation of adipocytes. Further experiments are required to determine if this generates a more accurate measurement of adipocyte cell area and volume. Alternatively, the same limitation or difficulty in distinguishing individual adipocyte membranes may remain a challenge.

7.5 Limitations of “stitching” in assessing collagen content

Histological analysis of lymphoedema and normal AT sections showed areas with extensive collagen content (Figure 3). Due to the randomness of the collagen, it was not possible to obtain images from different fields of view that were representative of the collagen content in each patient sample. For this reason, a “stitching” plugin in ImageJ (Preibisch et al., 2009) was used to reconstruct an image of the entire AT section from individual images, using an image overlap of 20%. Stitching was performed using a 10X objective. A 4X objective could have also been used, and hence fewer images would have needed to be taken. However, a 4X objective lens has a numerical aperture of 0.2, and as a result the image will lose resolution. It was found that stitching was not always able to create the correct output image. For example, images that did not contain much tissue or collagen, but lots of space, were not stitched into the correct position. Also, given the honeycomb-like structure of AT, stitching could not

differentiate between certain images containing similar AT morphology, and as a result these images were stitched into random areas. Incorrect and random stitching was also encountered when the images were stitched manually by joining images one at a time. To overcome this, the images that could not be stitched into its correct position were simply not included in the analysis. As a result, there is variation in the areas of the final stitched images (Figure 11, 12), and therefore the extent of collagen content in each patient sample could not always be accurately determined – although it does appear to be an accurate method for contiguous areas that are successfully imaged and stitched together. Nevertheless, this creates a problem: a stitched image that covers a greater area will have a greater degree of collagen deposition than a stitched image that covers a smaller area (Figure 11, 12). This is evident in the graph of the proportion of collagen content (Figure 13), where the data points for secondary lymphoedema and normal patients are all scattered. Therefore, a more sensitive image analysis technique must be developed to accurately estimate the proportion of collagen present.

7.6 Optimization of immunohistochemical methods

AT is largely comprised of adipocytes containing large lipid droplets, which makes them highly fragile. Consequently, we found that much of the structural integrity of lymphoedema AT is lost when it is processed and sectioned for histological analysis. This hindered our immunostaining methods, with numerous attempts at IHC resulting in a lack of target staining in lymphoedema AT and positive control tissues. For example, a change in detection system from a secondary goat anti-mouse IgG-HRP antibody (R&D Systems) to a goat anti-mouse IgG biotinylated secondary antibody (DAKO) made no difference, with no positive staining detected in the positive control tissue in the initial IHC attempts (Figure 16). It was possible that the primary antibody had lost reactivity, however, the primary antibodies were newly purchased and stored correctly, and the concentrations used in each IHC optimization test was equal to or higher than what has been previously described (Aron-Wisnewsky et al., 2009; Divoux et al., 2010). An external optimization test conducted by Mr. Rowan Ikin (Kolling Institute, St Leonards, New South Wales) revealed that a change to DAKO reagents was necessary to detect positive staining. This included changing the wash buffer from phosphate buffered saline (PBS) to a buffer consisting of 0.1% Tween 20 diluted into tris-buffered saline (TBST), since this detergent is known to decrease background staining and enhance reagent spreading. An antigen retrieval kit from R&D Systems was changed to a DAKO EnVisionTM FLEX target retrieval solution, high pH, since external tests showed positive staining when this antigen retrieval system was employed (Figure 17). Furthermore, external tests showed that compared to water-bath heating, antigen retrieval by microwave heating had a few disadvantages. The distribution of heat within a microwave is frequently inconsistent, resulting in a lack of reproducibility with respect to staining intensities. Also, the agitating action from the boiling antigen retrieval solution can lead to tissue detachment from the slides. Therefore, because of the uniform and consistent heat distribution it produces, antigen unmasking was performed by water-bath heating. Finally, the detection system was changed from a secondary goat anti-mouse IgG HRP conjugated antibody (R&D Systems) to a mouse IgG labeled polymer-HRP secondary antibody (DAKO), since this secondary antibody has been shown to amplify signal intensity up to 20 times greater without increasing background staining (Heras et al., 1995).

7.7 Cellular composition of lymphoedema AT and normal AT is the same

AT is distributed throughout the body in a variety of locations (Trujillo and Scherer, 2006). Subsequently, these adipose depots may vary across all aspects of AT structure and composition. Statistical comparisons were therefore made between the same anatomical

structures, lymphoedema arm versus normal arm and lymphoedema leg versus normal leg, in order to determine statistically significant differences that are biologically relevant. This analysis indicated that there is no significant difference in the cellular composition of lymphoedema AT compared with normal AT – when comparing tissue from the same limb type (arms or legs). It was postulated that adipocyte cell number and adipocyte size would be greatest in lymphoedema patients compared to normal individuals, since the progressive accumulation of static lymph fluid in lymphoedema correlates with AT accumulation, exacerbating swelling of the affected limb, and maximally expanding the affected area in size (Szuba and Rockson, 1998; Rockson, 2001; Warren et al., 2007). Our results were not able to support this hypothesis, with only a significant difference found in mean adipocyte number in AT from normal legs compared with AT from lymphoedema legs ($P < 0.05$). This is somewhat surprising given that in obese humans, it is known that AT expansion may be due to enlargement of existing fat cells (adipocytes), and/or to an increase in the total number of adipocytes (Arner et al., 2010; Sun et al., 2011). It is possible that patients having liposuction for non-medical reasons may themselves have an underlying metabolic syndrome that we are not aware of, given that we did not have access to their clinical information. The ideal liposuction candidates for our AT tissue donors (controls) are healthy individuals who do not have a life-threatening illness or medical condition, and individuals within 30% of their ideal weight who have firm, elastic skin and good muscle tone (Lanzer, 2002). Nevertheless, normal AT liposuction tissue is difficult to acquire and we are fortunate to have these tissue samples for comparison in our research. Further clinical background information (with HREC approval) is currently being sought for the normal AT liposuction donors.

It was also postulated that connective fibers and immune cells will be present in lymphoedema AT, since these cell types have been shown to be present in the AT of obese individuals (Khan et al., 2009). We showed that in lymphoedema AT, there are areas of extensive collagen content and abundant perivascular fibrosis, extending throughout the tissue (Figure 3). Surprisingly, there was also abundant areas of collagen content in normal AT (Figure 11, 12). However, because of the limitations in the stitching analysis performed, meaningful comparisons between the proportion of collagen content in lymphoedema AT and normal AT cannot be made. Moreover, perivascular collagen was found to be abundant around CD31 positive blood vessels (Figure 20). Although, an optimization test on DAKO reagents did show positive staining for CD31 and podoplanin (lymphatic endothelial cells) (Figure 18), the podoplanin staining could not be replicated on subsequent IHC experiments (Figure 21, 22). Therefore, further optimization of IHC methods are necessary in order to detect podoplanin positive lymphatic endothelial cells. Despite this, since only some vessels stained for CD31 and other adjacent vessels were negative, it is extremely likely that the negative vessels are lymphatic vessels, given that there are only two types of vessels, blood or lymph vessels.

7.8 The role of collagen in AT remodelling

Under normal circumstances, AT is considered a connective tissue of low density and high plasticity. However, we have demonstrated that in lymphoedema, there is connective tissue overgrowth, especially around vessels and extending throughout the tissue, due to an abundance of collagen (Figure 3A(iv-vi), 3B(iv-vi)). This mirrors AT from obese humans, which is characterized by an increase in fibrosis and increases in components of the extracellular matrix (ECM), including collagen (Pasarica et al., 2009; Spencer et al., 2010). As the collagen content increases, the overall rigidity of AT also increases, likely contributing to an increase in its mechanical strength (Scherer et al., 1998b).

The term “fibrosis” has been defined as the formation of fibrous tissue as a reparative or reactive process, which has been widely utilized in the context of the liver, lung, and kidney, in addition to several other tissues (Khan et al., 2009). In obese AT, fibrosis appears to be initiated in response to adipocyte hypertrophy, which occurs as the initial step toward fat mass expansion through enlargement of the lipid droplet size in existing adipocytes (Khan et al., 2009). This cellular expansion seems to constitute the initial insult, in response to which the up regulation of ECM components is triggered (Khan et al., 2009). Similar processes are likely to occur in lymphoedema, given that liposuction-derived AT from lymphoedema patients show adipocyte hypertrophy with an enhanced fibrotic response that includes extensive collagen deposition (Figure 3A(iv-vi), 3B(iv-vi)).

With AT hypertrophy, considerable tissue remodeling is required, involving stromal cells, pre-adipocytes, endothelial cells, and immune cells (Spencer et al., 2011). Adipocytes are embedded in a dense network of ECM (Napolitano, 1963). The ECM not only functions to provide mechanical support for a fat mass, but also regulates the physiological and pathological events of AT remodeling through a variety of signaling pathways (Khan et al., 2009). During AT expansion in the obese state, the ECM actively remodels to accommodate the adipocyte growth. This includes the up regulation of several ECM components, including collagen (Khan et al., 2009; Sun et al., 2011). The nature and consequences of ECM modification in AT have been mostly investigated in mice. In obese mice, various types of collagen are overexpressed in the AT (Khan et al., 2009). The predominantly expressed collagens are types I, IV, and VI. In collagen VI-null obese mice, the lack of collagen VI associates with increased adipocyte size (Liu et al., 2009). A similar phenotype of adipose cell hypertrophy was reported in secreted acidic cysteine-rich glycoprotein (SPARC), a matricellular glycoprotein implicated in the synthesis of ECM components (Bradshaw et al., 2003). These observations suggest that increased ECM deposition in AT may contribute to restrain adipocyte expansion in obesity. Thus, the ECM in AT is dysfunctional in obesity and contributes to the metabolic syndrome (Scherer et al., 1998b; Khan et al., 2009). However, the extent of ECM remodeling in lymphoedema is unknown and further research is required in this area.

The ECM contains multiple types of collagen including I, IV, V, VI, VII, VIII, and IX; among these collagen VI is highly enriched in the ECM of AT (Scherer et al., 1998b). PSR polarizing light microscopy showed type III collagen is abundant in human lymphoedema AT (Figure 2A(vi), 2B(vi); color image not available). Type III collagen is a member of the fibrillar collagen family comprising three α1 chains. It is co-localized with the most abundant member of the collagen family, type I collagen, in such tissues as blood vessels and skin (Liu et al., 1997; Trikka et al., 1997). Thus, the ECM in lymphoedema AT accumulates high levels of fibrillar collagen, particularly around blood vessels.

Whether type VI collagen is also present in lymphoedema AT is currently unknown. Collagen VI α3-subunit (COL6A3) expression has been shown to increase in human obesity (Pasarica et al., 2009). For example, it has been shown that the expression of collagen VI in human AT is upregulated in moderately obese indviduals, and that obese individuals with elevated collagen VI display increased AT inflammation (Pasarica et al., 2009). While weakening of the ECM that surrounds AT by elimination of collagen VI leads to improved survival rates of adipocytes and improvements in metabolism (Khan et al., 2009). This suggests that increased collagen VI deposition could be a hallmark of AT deregulation in obesity. Hence, it is likely that collagen VI is also present in lymphoedema AT, since it is abundantly produced and secreted by adipocytes (Scherer et al., 1998a). Collagen VI is

composed of 3 chains, α1, α2, and α3, which associate to form higher-order complexes (Baldock et al., 2003). Collagen VI contributes essential functions to the local ECM environment by providing structural support for cells and enrichment of growth factors, cytokines, and other ligands on cell surfaces and, in fact, can itself assume important signaling effects (Vogel, 2001). A future experiment that might be informative is to stain for collagen VI in liposuction-derived lymphoedema AT, using an antibody that binds to the α3 chain of the human collagen VI (Divoux et al., 2010), to confirm its presence in human lymphoedema AT. Therefore, collagen III and possibly additional extracellular matrix components are extremely important in modulating adipocyte physiology.

Fibrosis and the deposition of ECM can also affect the angiogenic properties of tissues. Once endothelial cells begin sprouting, a number of ECM proteins must be degraded to allow vessel extension (Spencer et al., 2011). In lymphoedema AT, collagen was found to surround blood vessels. The association of collagen III with blood vessels and in fibrotic areas is currently unknown. However, collagen V, which is also a form of fibrillar collagen has been shown to be abundant in fibrotic areas as well as in large blood vessels in obese individuals (Spencer et al., 2011). The strong association of collagen V with larger blood vessels and in fibrotic areas is interesting because of the known association of collagen V with vascular function (Spencer et al., 2011). In fact, previous studies have suggested that collagen V may inhibit endothelial cell adherence to the basement membrane substrate and impair endothelial migration (Yamamoto et al., 1992; Fichard et al., 1995), and collagen V is known to have a domain that binds thrombospondin, which is also anti-angiogenic (Mumby et al., 1984). Furthermore, there is an association between collagen V and scleroderma, which is characterized by intense fibrosis and microvascular occlusion (Mumby et al., 1984). Therefore, the increase vascular collagen V in obese AT or lymphoedematous AT may impair angiogenesis, and also possibly lymphangiogenesis.

7.9 Role of Transforming Growth Factor β in fibrosis

As indicated above, there is minimal knowledge about the processes of fibrosis in lymphoedema. This process is likely to depend on the pro-fibrotic cytokine, Transforming Growth Factor β (TGFβ), which contributes to fibrosis of several tissues, by increasing expression of matrix components, such as collagens (I, III, IV), fibronectin, and matrix proteolgycans, and by inducing inhibitors of matrix-degrading matrix metalloproteinases (MMPs) (Branton and Kopp, 1999). Furthermore, given that Mφ express high levels of TGFβ and Mφ-like cells are highly abundant in lymphoedema AT (Figure 3A(ii,iii), 3B(ii,iii)), it is possible that fibrosis involves Mφ and Mφ-derived TGF-β. Initial IHC optimization tests could not detect positive staining for TGFβ. Once optimized, a future experiment should be to perform IHC to detect the presence of TGFβ in lymphoedema versus normal AT. This was not possible in the present study due to time constraints of the Masters of Research program.

7.10 Macrophages in AT

Increased Mφ accumulation in expanding AT has been described both in obese mice and humans (Weisberg et al., 2003; Xu et al., 2003; Aron-Wisnewsky et al., 2009; Divoux et al., 2010). However, it is not known whether Mφ are similarly abundant in normal or lymphoedema AT, and if they play a similar role to adipose tissue macrophages (ATMs) as they do in obesity. Indeed, our initial histological analysis of human lymphoedema AT indicates the presence of abundant cells (leukocytes) that morphologically resemble tissue Mφ (Figure 3A(ii,iii), 3B(ii,iii)). However, we were not able to determine the identity of these Mφ-like cells with no positive staining detected for HAM56 Mφ antigen (Figure 23).

Although, no positive staining was detected in the positive control liver tissue (Figure 23). This is surprising because HAM56 exclusively reacts with two populations of cells: fixed tissue Mφ, for example, "tingible Mφ" and interdigitating Mφ of lymph nodes, and tissue Mφ including Kupffer cells of the liver and alveolar Mφ of the lung; and a subpopulation of endothelial cells, most prominently those of the capillaries and smaller blood vessels (Gown et al., 1986). More work is required to better optimize IHC detection with the HAM56 antibody, or another antibody specific to another Mφ-specific antigen, for example, CD11b (Weisberg et al., 2006). M1-specific antigens (e.g. CD40) and M2-specific markers (e.g. CD206) should be included in future IHC staining experiments, to determine the identity of the Mφ-like cells in lymphoedema AT. Indeed, initial optimization tests did include these markers, however, due to time constraints it was not possible to test these markers with the DAKO detection system.

7.11 Macrophages: master regulators of inflammation

The association of adipocyte hypertrophy with increased Mφ recruitment, in obesity, has led to the current idea that an increase in adipocyte size is indicative of inflammation in AT, and is generally associated with an unfavorable metabolic profile (Khan et al., 2009). The AT of obese mice and humans are prone to secrete large quantities of pro-inflammatory cytokines, chemokines, and peptides including TNF-α, TGF-β, IL-6, monocyte chemoattractant protein-1 (MCP-1), and leptin (Skurk et al., 2007) – all of which are able to recruit and stimulate cells of the immune system. Many of these pro-inflammatory mediators also have documented angiogenic activity (Leibovich et al., 1987; Sierra-Honigmann et al., 1998); or are able to indirectly stimulate angiogenesis via promoting the production of angiogenic growth factors from adipocytes or Mφ (Rega et al., 2007). Mφ have been shown to produce lymphangiogenic growth factors including vascular endothelial growth factors A, C and D (VEGF-A, -C, -D) in response to inflammatory stimuli (Berse et al., 1992; Schoppmann et al., 2002; Cursiefen et al., 2004). Mφ have also been demonstrated to promote lymphangiogenesis in mouse models of inflammatory disease (Schoppmann et al., 2002; Cursiefen et al., 2004) and to stimulate angiogenesis in epididymal AT (Cho et al., 2007). It is therefore plausible that obesity-stimulated and lymphoedema-stimulated inflammation is able to promote both angiogenesis and lymphangiogenesis within AT.

Adipocyte hypertrophy can also lead to necrosis-like adipocyte death (Cinti et al., 2005). Cell contents are released in the extracellular space where they are thought to trigger inflammatory responses from Mφ recruited to the AT to scavenge the resulting cell debris. These Mφ also tend to accumulate around necrotic adipocytes to form crown-like structures in advanced obesity (Cinti et al., 2005). In this state, they phagocytose the residual lipid droplet, forming large lipid-laden multinucleated syncytia in the process, a commonly accepted hallmark of chronic inflammation (Cinti et al., 2005; Lumeng et al., 2007). Thus, adipocyte hypertrophy and its related perturbed biology could be directly involved in the development of chronic low-grade inflammation by secreting pro-inflammatory molecules and/or liberating intracellular components after death. In lymphoedema AT, no crown-like structures have been observed in our analysis to date. Further research is required to determine if these initial observations are true in a larger sample cohort, since there are plenty of Mφ-like cells present throughout the AT, mostly located through connective tissue regions, in close proximity with collagen (Figure 3A(ii,iii), 3B(ii,iii)).

In conclusion, this is the first study to characterize the AT removed through liposuction surgery, from lymphoedema patients. Using ImageJ processing software, we developed a microscopic image analysis method to estimate adipocyte cell number, size, and collagen

content. We found that overall, adipocyte cell number, size, and the extent of collagen content was similar in lymphoedema AT and normal AT, with only a significant difference found in mean adipocyte number in AT from normal legs compared with AT from lymphoedema legs ($P < 0.05$). Furthermore, we identified perivascular collagen localization around blood vessels, which may play a role in angiogenesis, and also possibly lymphangiogenesis. More work is however required to better optimize IHC detection of podoplanin positive lymphatic endothelial cells, and to determine the identity of the Mφ-like cells in lymphoedema to identify their role (if any) in fibrosis and inflammation. Taken together, the data presented in this thesis concludes that the pathophysiological features that are well documented in obese AT, including adipocyte hypertrophy, hyperplasia, ECM overproduction, and increased connective fiber content, appears to also occur in lymphoedema AT.

8. Acknowledgments

First and foremost, I would like to take this opportunity to thank my supervisor, Dr. Lisa Sedger who essentially has made all this possible. I am indebted for all her invaluable advice, encouragement, patience and never-ending enthusiasm in guiding me throughout my Masters candidature.

My sincere thanks also goes to Dr. Michael Johnson for his help and support throughout the year. I would also like to thank Rowan Ikin for getting the IHC up and running and providing us with the positive control tissue. Dr. Suha Kilani for allowing us access to her lab's polarizing light microscope. Dr Daniel Lanzer's clinic, particularly Ange Denning, for providing us with the normal liposuction samples.

Thank you to the Lymphoedema group, Dr. Thomas Lam and Dr. Quan Ngo who performed the liposuction surgeries, Katrina Kastanias for providing the clinic data.

Of course, my roller coaster journey would not have been made possible if without the support from my fellow MRes colleagues.

Most importantly, I thank my family who have always been by my side, for their constant encouragement and love. To Mum and Dad, Mervin, Pilar, and Belle, thank you for always being there for me, ensuring my sanity is well checked.

We thank Macquarie Medical Imaging and Macquarie University Cancer Institute for its financial support.

Macquarie University HREC approval: Protocol 5201300315

9. Other Contributors

The Histopathology Laboratory, Department of Pathology, The University of Sydney for paraffin embedding and processing for histological analysis.

Mr. Rowan Ikin, Kolling Institute of Medical Research (St Leonards, New South Wales) for optimizing IHC staining.

10. References

Ahima, R.S., and Flier, J.S. (2000). Adipose tissue as an endocrine organ. *Trends Endocrinol. Metab.* 11**,** 327-332.

Ailhaud, G. (2001). Development of white adipose tissue and adipocyte differentiation. *Adipose tissue. Diabetes*. 14, 27-54.

Ailhaud, G., Grimaldi, P., and Negrel, R. (1992). Cellular and molecular aspects of adipose tissue development. *Annu. Rev. Nutr.* 12**,** 207-233.

Arner, E., Westermark, P.O., Spalding, K.L., Britton, T., Rydén, M., Frisén, J., Bernard, S., and Arner, P. (2010). Adipocyte turnover: relevance to human adipose tissue morphology. *Diabetes.* 59**,** 105-109.

Aron-Wisnewsky, J., Tordjman, J., Poitou, C., Darakhshan, F., Hugol, D., Basdevant, A., Aissat, A., Guerre-Millo, M., and Clement, K. (2009). Human adipose tissue macrophages: m1 and m2 cell surface markers in subcutaneous and omental depots and after weight loss. *J. Clin. Endocrinol. Metab.* 94**,** 4619-4623.

Baldock, C., Sherratt, M.J., Shuttleworth, C.A., and Kielty, C.M. (2003). The supramolecular organization of collagen VI microfibrils. *J. Mol. Biol.* 330**,** 297-307.

Bell, R., Brice, G., Child, A., Murday, V., Mansour, S., Sandy, C., Collin, J., Brady, A., Callen, D., and Burnand, K. (2001). Analysis of lymphoedema-distichiasis families for FOXC2 mutations reveals small insertions and deletions throughout the gene. *Hum. Genet.* 108**,** 546-551.

Bełtowski, J. (2003). Adiponectin and resistin—new hormones of white adipose tissue. *Med. Sci. Monit.* 9**,** 61.

Berse, B., Brown, L.F., Van De Water, L., Dvorak, H.F., and Senger, D.R. (1992). Vascular permeability factor (vascular endothelial growth factor) gene is expressed differentially in normal tissues, macrophages, and tumors. *Mol. Biol. Cell.* 3**,** 211-220.

Bradshaw, A., Graves, D., Motamed, K., and Sage, E. (2003). SPARC-null mice exhibit increased adiposity without significant differences in overall body weight. *Proc. Natl. Acad. Sci.* 100**,** 6045-6050.

Branton, M.H., and Kopp, J.B. (1999). TGF-β and fibrosis. *Microbes Infect.* 1**,** 1349-1365.

Brorson, H. (2003). Liposuction in arm lymphedema treatment. *Scan. J. Surg.* 92**,** 287-295.

Brorson, H., and Svensson, H. (1998). Liposuction combined with controlled compression therapy reduces arm lymphedema more effectively than controlled compression therapy alone. *Plast. Reconstr. Surg.* 102**,** 1058-1067.

Cancello, R., Henegar, C., Viguerie, N., Taleb, S., Poitou, C., Rouault, C., Coupaye, M., Pelloux, V., Hugol, D., and Bouillot, J. L. (2005). Reduction of macrophage infiltration and

chemoattractant gene expression changes in white adipose tissue of morbidly obese subjects after surgery-induced weight loss. *Diabetes.* 54**,** 2277-2286.

Cho, C.-H., Koh, Y.J., Han, J., Sung, H.-K., Lee, H.J., Morisada, T., Schwendener, R.A., Brekken, R.A., Kang, G., and Oike, Y. (2007). Angiogenic role of LYVE-1–positive macrophages in adipose tissue. *Circulation research* 100**,** e47-e57.

Cinti, S., Mitchell, G., Barbatelli, G., Murano, I., Ceresi, E., Faloia, E., Wang, S., Fortier, M., Greenberg, A.S., and Obin, M.S. (2005). Adipocyte death defines macrophage localization and function in adipose tissue of obese mice and humans. *J. Lipid Res.* 46**,** 2347-2355.

Cristancho, A.G., and Lazar, M.A. (2011). Forming functional fat: a growing understanding of adipocyte differentiation. *Nat. Rev. Mol. Cell Biol.* 12**,** 722-734.

Cursiefen, C., Chen, L., Borges, L.P., Jackson, D., Cao, J., Radziejewski, C., D'amore, P.A., Dana, M.R., Wiegand, S.J., and Streilein, J.W. (2004). VEGF-A stimulates lymphangiogenesis and hemangiogenesis in inflammatory neovascularization via macrophage recruitment. *J. Clin. Invest.* 113**,** 1040-1050.

Dandona, P., Aljada, A., and Bandyopadhyay, A. (2004). Inflammation: the link between insulin resistance, obesity and diabetes. *Trends Immunol.* 25**,** 4-7.

Disipio, T., Rye, S., Newman, B., and Hayes, S. (2013). Incidence of unilateral arm lymphoedema after breast cancer: a systematic review and meta-analysis. *Lancet Oncol.* 14**,** 500-515.

Divoux, A., Tordjman, J., Lacasa, D., Veyrie, N., Hugol, D., Aissat, A., Basdevant, A., Guerre-Millo, M., Poitou, C., and Zucker, J.-D. (2010). Fibrosis in human adipose tissue: composition, distribution, and link with lipid metabolism and fat mass loss. *Diabetes.* 59**,** 2817-2825.

Drury, R.B., and Wallington, E. (1967). *Carleton's histological technique.* New York: Oxford University Press.

Ellis, S. (2006). Structure and function of the lymphatic system: an overview. *Br. J. Community Nurs.* 11**,** S4-S6.

Fang, J., Dagenais, S.L., Erickson, R.P., Arlt, M.F., Glynn, M.W., Gorski, J.L., Seaver, L.H., and Glover, T.W. (2000). Mutations in FOXC2 (MFH-1), a forkhead family transcription factor, are responsible for the hereditary lymphedema-distichiasis syndrome. *Am. J. Hum. Genet.* 67**,** 1382-1388.

Fichard, A., Kleman, J.-P., and Ruggiero, F. (1995). Another look at collagen V and XI molecules. *Matrix Biol.* 14**,** 515-531.

Finegold, D.N., Kimak, M.A., Lawrence, E.C., Levinson, K.L., Cherniske, E.M., Pober, B.R., Dunlap, J.W., and Ferrell, R.E. (2001). Truncating mutations in FOXC2 cause multiple lymphedema syndromes. *Hum. Mol. Genet.* 10**,** 1185-1189.

Fjeldborg, K., Pedersen, S.B., Møller, H.J., Christiansen, T., Bennetzen, M., and Richelsen, B. (2014). Human adipose tissue macrophages are enhanced but changed to an anti-inflammatory profile in obesity. *J. Immunol. Res.* 309548, 1-10.

Foldi, E. (1998). The treatment of lymphedema. *Cancer.* 83**,** 2833-2834.

Frühbeck, G., Gómez-Ambrosi, J., Muruzábal, F.J., and Burrell, M.A. (2001). The adipocyte: a model for integration of endocrine and metabolic signaling in energy metabolism regulation. *Am. J. Physiol. Endocrinol. Metab.* 280**,** 827-847.

Gaffney, R., and Casley-Smith, J. (1981). Excess plasma proteins as a cause of chronic inflammation and lymphoedema: biochemical estimations. *J. Path.* 133**,** 229-242.

Gesta, S., Tseng, Y.-H., and Kahn, C.R. (2007). Developmental origin of fat: tracking obesity to its source. *Cell.* 131**,** 242-256.

Gordon, K.D., and Mortimer, P.S. (2007). A guide to lymphedema. *Exp. Rev. Derm.* 2**,** 741-752.

Gown, A.M., Tsukada, T., and Ross, R. (1986). Human atherosclerosis. II. Immunocytochemical analysis of the cellular composition of human atherosclerotic lesions. *Am. J.Path.* 125**,** 191.

Gray, P. (1954). The microtomist's formulary and guide. *The Miorotomist's Formulary and Guide.*

Halberg, N., Wernstedt-Asterholm, I., and Scherer, P.E. (2008). The adipocyte as an endocrine cell. *Endocrinol. Metab. Clin. North Am.* 37**,** 753-768.

Harvey, N.L., Srinivasan, R.S., Dillard, M.E., Johnson, N.C., Witte, M.H., Boyd, K., Sleeman, M.W., and Oliver, G. (2005). Lymphatic vascular defects promoted by Prox1 haploinsufficiency cause adult-onset obesity. *Nat. Genet.* 37**,** 1072-1081.

Heras, A., Roach, C., and Key, M. (Year). Enhanced polymer detection system for immunohistochemistry, in: *Laboratory Investigation.* Williams & Wilkins 351 West Camden St, Baltimore.

Hinrichs, C.S., Watroba, N.L., Rezaishiraz, H., Giese, W., Hurd, T., Fassl, K.A., and Edge, S.B. (2004). Lymphedema secondary to postmastectomy radiation: incidence and risk factors. *Ann. Surg. Oncol.* 11**,** 573-580.

Irrthum, A., Devriendt, K., Chitayat, D., Matthijs, G., Glade, C., Steijlen, P.M., Fryns, J.P., Van Steensel, M.A., and Vikkula, M. (2003). Mutations in the transcription factor gene SOX18 underlie recessive and dominant forms of hypotrichosis-lymphedema-telangiectasia. *Am. J. Hum. Genet.* 72**,** 1470-1478.

Irrthum, A., Karkkainen, M.J., Devriendt, K., Alitalo, K., and Vikkula, M. (2000). Congenital hereditary lymphedema caused by a mutation that inactivates VEGFR3 tyrosine kinase. *Am. J. Hum. Genet.* 67**,** 295-301.

Junqueira, L.C., Bignolas, G., and Brentani, R. (1979). Picrosirius staining plus polarization microscopy, a specific method for collagen detection in tissue sections. *Histochem. J.* 11**,** 447-455.

Karkkainen, M.J., Ferrell, R.E., Lawrence, E.C., Kimak, M.A., Levinson, K.L., Mctigue, M.A., Alitalo, K., and Finegold, D.N. (2000). Missense mutations interfere with VEGFR-3 signalling in primary lymphoedema. *Nat. Genet.* 25**,** 153-159.

Katz, A.J. (2002). Mesenchymal cell culture: adipose tissue. *Methods of Tissue Engineering.* New York: Academic Press**,** 277-286.

Khan, T., Muise, E.S., Iyengar, P., Wang, Z.V., Chandalia, M., Abate, N., Zhang, B.B., Bonaldo, P., Chua, S., and Scherer, P.E. (2009). Metabolic dysregulation and adipose tissue fibrosis: role of collagen VI. *Mol. Cell Biol.* 29**,** 1575-1591.

Kiernan, J.A. (1999). Histological and histochemical methods: theory and practice. *Shock.* 12**,** 479.

Lagathu, C., Yvan-Charvet, L., Bastard, J.-P., Maachi, M., Quignard-Boulange, A., Capeau, J., and Caron, M. (2006). Long-term treatment with interleukin-1β induces insulin resistance in murine and human adipocytes. *Diabetologia.* 49**,** 2162-2173.

Lanzer, D. (2002). Safety of Large-Volume Liposuction. *Int. J. Cosmet. Surg. Aesth. Dermatol.* 4**,** 173-177.

Leibovich, S.J., Polverini, P.J., Shepard, H.M., Wiseman, D.M., Shively, V., and Nuseir, N. (1987). Macrophage-induced angiogenesis is mediated by tumour necrosis factor-α. *Nature.* 329**,** 630-632.

Liu, J., Divoux, A., Sun, J., Zhang, J., Clément, K., Glickman, J.N., Sukhova, G.K., Wolters, P.J., Du, J., and Gorgun, C.Z. (2009). Genetic deficiency and pharmacological stabilization of mast cells reduce diet-induced obesity and diabetes in mice. *Nat. Med.* 15**,** 940-945.

Liu, X., Wu, H., Byrne, M., Krane, S., and Jaenisch, R. (1997). Type III collagen is crucial for collagen I fibrillogenesis and for normal cardiovascular development. *Proc. Natl. Acad. Sci.* 94**,** 1852-1856.

Lumeng, C.N., Deyoung, S.M., Bodzin, J.L., and Saltiel, A.R. (2007). Increased inflammatory properties of adipose tissue macrophages recruited during diet-induced obesity. *Diabetes.* 56**,** 16-23.

Meige, H. (1898). *Dystrophie oedemateuse hereditaire*. Presse méd 6**.**

Milroy, W.F. (1892). *An undescribed variety of hereditary oedema.* Appleton.

Mumby, S.M., Raugi, G.J., and Bornstein, P. (1984). Interactions of thrombospondin with extracellular matrix proteins: selective binding to type V collagen. *J. Cell Biol.* 98**,** 646-652.

Napolitano, L. (1963). The differentiation of white adipose cells an electron microscope study. *J. Cell Biol.* 18**,** 663-679.

Nishimura, S., Manabe, I., Nagasaki, M., Hosoya, Y., Yamashita, H., Fujita, H., Ohsugi, M., Tobe, K., Kadowaki, T., and Nagai, R. (2007). Adipogenesis in obesity requires close interplay between differentiating adipocytes, stromal cells, and blood vessels. *Diabetes.* 56**,** 1517-1526.

Nougues, J., Reyne, Y., and Dulor, J.-P. (1988). Differentiation of rabbit adipocyte precursors in primary culture. *Int. J. Obes.* 12**,** 321-333.

Nwaneshiudu, A., Kuschal, C., Sakamoto, F.H., Anderson, R.R., Schwarzenberger, K., and Young, R.C. (2012). Introduction to confocal microscopy. *J. Invest. Derm.* 132**,** 513-518.

Ozaslan, C., and Kuru, B. (2004). Lymphedema after treatment of breast cancer. *Am. J. Surg.* 187**,** 69-72.

Pasarica, M., Gowronska-Kozak, B., Burk, D., Remedios, I., Hymel, D., Gimble, J., Ravussin, E., Bray, G.A., and Smith, S.R. (2009). Adipose tissue collagen VI in obesity. *J. Clin. Endocrinol. Metab.* 94**,** 5155-5162.

Preibisch, S., Saalfeld, S., and Tomancak, P. (2009). Globally optimal stitching of tiled 3D microscopic image acquisitions. *Bioinformatics.* 25**,** 1463-1465.

Rega, G., Kaun, C., Demyanets, S., Pfaffenberger, S., Rychli, K., Hohensinner, P., Kastl, S., Speidl, W., Weiss, T., and Breuss, J. (2007). Vascular endothelial growth factor is induced by the inflammatory cytokines interleukin-6 and oncostatin m in human adipose tissue in vitro and in murine adipose tissue in vivo. *Arterioscl. Throm. Vas. Biol.* 27**,** 1587-1595.

Rockson, S.G. (2001). Lymphedema. *Am. J. Med.* 110**,** 288-295.

Rosen, E.D., and Macdougald, O.A. (2006). Adipocyte differentiation from the inside out. *Nat. Rev. Mol. Cell Biol.* 7**,** 885-896.

Ruifrok, A.C., and Johnston, D.A. (2001). Quantification of histochemical staining by color deconvolution. *Anal. Quant. Cytol.* 23**,** 291-299.

Rutkowski, J.M., Davis, K.E., and Scherer, P.E. (2009). Mechanisms of obesity and related pathologies: The macro- and microcirculation of adipose tissue. *Fed. Europe. Biochem. Soc.* 276**,** 5738-5746.

Ryan, T.J. (1995). Lymphatics and adipose tissue. *Clin. Dermatol.* 13**,** 493-498.

Schacht, V., Ramirez, M.I., Hong, Y.K., Hirakawa, S., Feng, D., Harvey, N., Williams, M., Dvorak, A.M., Dvorak, H.F., and Oliver, G. (2003). T1α/podoplanin deficiency disrupts normal lymphatic vasculature formation and causes lymphedema. *EMBO J.* 22**,** 3546-3556.

Scherer, P., Bickel, P., Kotler, M., and Lodish, H. (1998a). Subtractive antibody screening: a new method to clone cell-specific secreted and surface proteins. *Nat. Biotechnol.* 16**,** 581-586.

Scherer, P.E., Bickel, P.E., Kotler, M., and Lodish, H.F. (1998b). Cloning of cell-specific secreted and surface proteins by subtractive antibody screening. *Nat. Biotechnol.* 16**,** 581-586.

Schoppmann, S.F., Birner, P., Stöckl, J., Kalt, R., Ullrich, R., Caucig, C., Kriehuber, E., Nagy, K., Alitalo, K., and Kerjaschki, D. (2002). Tumor-associated macrophages express lymphatic endothelial growth factors and are related to peritumoral lymphangiogenesis. *Am. J. Path.* 161**,** 947-956.

Sierra-Honigmann, M.R.O., Nath, A.K., Murakami, C., García-Cardeña, G., Papapetropoulos, A., Sessa, W.C., Madge, L.A., Schechner, J.S., Schwabb, M.B., and Polverini, P.J. (1998). Biological action of leptin as an angiogenic factor. *Science.* 281**,** 1683-1686.

Skurk, T., Alberti-Huber, C., Herder, C., and Hauner, H. (2007). Relationship between adipocyte size and adipokine expression and secretion. *J. Clin. Endocrinol. Metab.* 92**,** 1023-1033.

Šmahel, J. (1986). Adipose tissue in plastic surgery. *Ann. Plas. Surg.* 16**,** 444-453.

Sun, K., Kusminski, C.M., and Scherer, P.E. (2011). Adipose tissue remodeling and obesity. *J. Clin. Invest.* 121**,** 2094-2101.

Szuba, A., and Rockson, S.G. (1998). Lymphedema: classification, diagnosis and therapy. *Vasc. Med.* 3**,** 145-156.

Trikka, D., Davis, T., Lapenta, V., Brahe, C., and Kessling, A. (1997). Human COL6A1: genomic characterization of the globular domains, structural and evolutionary comparison with COL6A2. *Mamm. Genome.* 8**,** 342-345.

Trujillo, M.E., and Scherer, P.E. (2006). Adipose tissue-derived factors: impact on health and disease. *Endocr. Rev.* 27**,** 762-778.

Vogel, W.F. (2001). Collagen-receptor signaling in health and disease. *Eur. J. Derm.* 11**,** 506-514.

Wang, Y., and Oliver, G. (2010). Current views on the function of the lymphatic vasculature in health and disease. *Genes Dev.* 24**,** 2115-2126.

Warren, A.G., Brorson, H., Borud, L.J., and Slavin, S.A. (2007). Lymphedema: a comprehensive review. *Ann. Plast. Surg.* 59**,** 464-472.

Weisberg, S.P., Hunter, D., Huber, R., Lemieux, J., Slaymaker, S., Vaddi, K., Charo, I., Leibel, R.L., and Ferrante Jr, A.W. (2006). CCR2 modulates inflammatory and metabolic effects of high-fat feeding. *J. Clin. Invest.* 116**,** 115-124.

Weisberg, S.P., Mccann, D., Desai, M., Rosenbaum, M., Leibel, R.L., and Ferrante, A.W. (2003). Obesity is associated with macrophage accumulation in adipose tissue. *J. Clin. Invest.* 112**,** 1796-1808.

Xu, H., Barnes, G.T., Yang, Q., Tan, G., Yang, D., Chou, C.J., Sole, J., Nichols, A., Ross, J.S., and Tartaglia, L.A. (2003). Chronic inflammation in fat plays a crucial role in the development of obesity-related insulin resistance. *J. Clin. Invest.* 112**,** 1821-1830.

Yamamoto, K., Yamamoto, M., and Noumura, T. (1992). Disassembly of F-actin filaments in human endothelial cells cultured on type V collagen. *Exp. Cell Res.* 201**,** 55-63.

Zuk, P.A., Zhu, M., Ashjian, P., De Ugarte, D.A., Huang, J.I., Mizuno, H., Alfonso, Z.C., Fraser, J.K., Benhaim, P., and Hedrick, M.H. (2002). Human adipose tissue is a source of multipotent stem cells. *Mol. Biol. Cell.* 13**,** 4279-4295.

Zuk, P.A., Zhu, M., Mizuno, H., Huang, J., Futrell, J.W., Katz, A.J., Benhaim, P., Lorenz, H.P., and Hedrick, M.H. (2001). Multilineage cells from human adipose tissue: implications for cell-based therapies. *Tissue Eng.* 7**,** 211-228.

Appendix A

Normality probability plots of adipocyte size for AT from **(A)** secondary lymphoedema arm; **(B)** normal arm; **(C)** secondary lymphoedema leg; **(D)** normal leg. All graphs show that the adipocyte size are normally distributed with points lying on or close to the straight line.

A

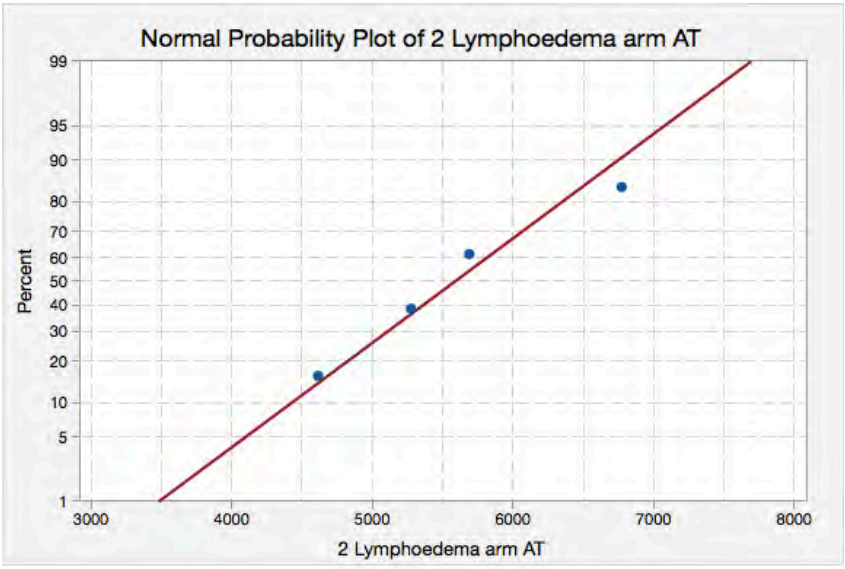

B

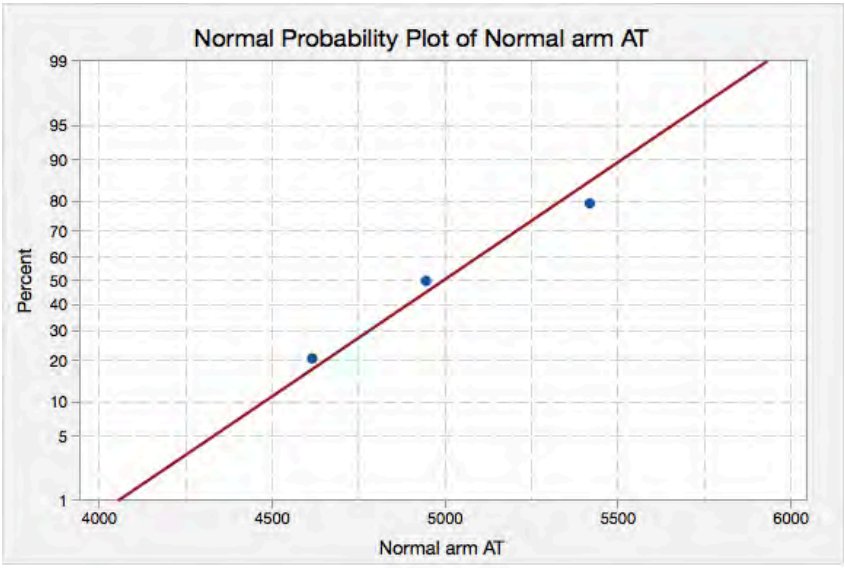

C

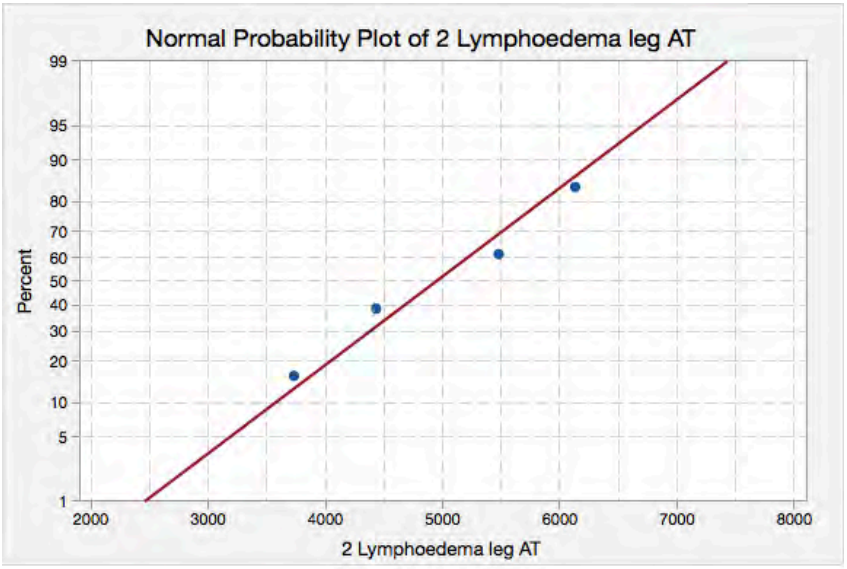
Normal Probability Plot of 2 Lymphoedema leg AT
Percent
99
95
90
80
70
60
50
40
30
20
10
5
1
2000
3000
4000
5000
6000
7000
8000
2 Lymphoedema leg AT

D

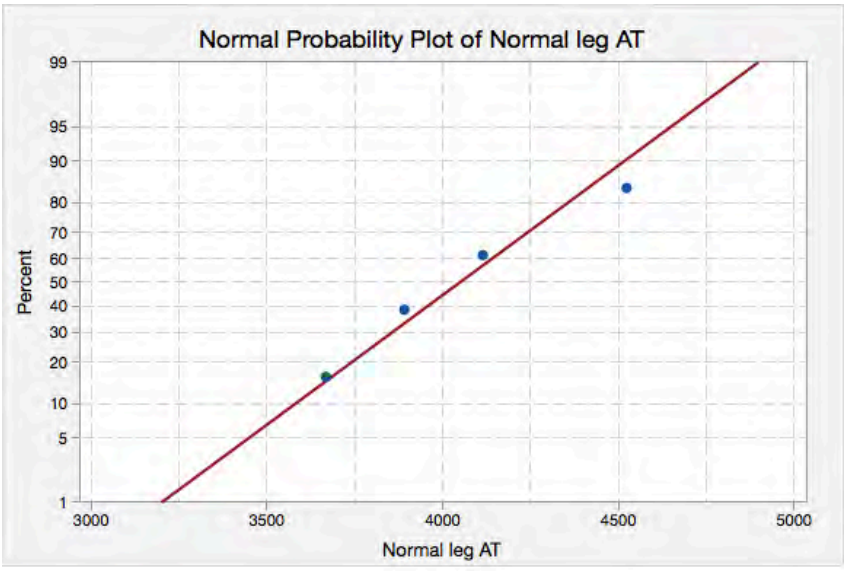
Normal Probability Plot of Normal leg AT
Percent
99
95
90
80
70
60
50
40
30
20
10
5
1
3000
3500
4000
4500
5000
Normal leg AT

Appendix B

Raw data of adipocyte cell number, adipocyte size, adipose tissue area, area of non-adipocyte cells, area of collagen. Showing values obtained for each of the six different fields of view. The area of collagen following "stitching" is also shown. (**A)** secondary lymphoedema arm AT; **(B)** normal arm AT; **(C)** secondary lymphoedema leg AT; **(D)** normal leg AT.

A

Lymphoedema arm AT												
	# adipocyte cells						**Adipocyte size (μm^2)**					
Patient sample												
BG	109	90	83	94	88	157	6038.6	5967.3	7664.4	4637.6	5200.1	4630.7
HM	126	166	133	73	95	84	5255.2	4174.2	3316.3	4105.2	5098.4	5740.3
PE	121	115	114	105	95	149	5138.5	5201.1	5777.3	5692.6	4788.5	5054.8
SP	93	114	125	101	90	105	6399.5	6699.0	8140.1	5557.3	6413.3	7427.5
MM	116	132	119	159	170	170	6890.3	5596.8	5511.2	3983.1	4146.6	5336.2

Lymphoedema arm AT													
	AT area (μm^2)						**Non-adipocyte cells (μm^2)**						**Collagen (μm^2)**
Patient sample													
BG	1072075.1	817280.3	1136300.5	1045790.3	1116747.2	1162926.9	412935.3	274988.2	498970.8	571692.4	639686.5	430717.7	1622161.6
HM	1075850.6	1125234.2	1026269.2	992356.3	965105.2	819777.2	412724.5	431885.9	578437.0	652408.9	480752.8	328594.4	1967356.4
PE	1031319.2	1117404.2	1028094.6	903708.9	1082942.5	1162622.9	314396.2	428267.2	423457.9	319189.1	571001.8	362744.1	259468.3
SP	1178850.5	1142270.9	1068585.0	1118203.9	1206032.9	1115531.0	482420.4	389919.9	364304.3	423122.4	580556.2	202268.7	552772.4
MM	1224831.5	1271278.8	1238271.5	1283224.6	1287032.0	1243465.1	422682.0	476279.9	512550.7	581579.5	579145.1	330662.8	2069942.5

B

Normal arm AT												
	# adipocyte cells						**Adipocyte size (μm^2)**					
Patient sample												
DL3	140	141	139	166	124	135	6212.8	4479.1	4962.9	4757.5	6263.9	5830.3
DL6	152	126	125	131	126	148	5067.1	4515.1	5251.3	6467.0	5499.3	5341.6
DL7	90	115	91	103	116	79						

Normal arm AT													
	AT area (μm^2)						**Non-adipocyte cells (μm^2)**						**Collagen (μm^2)**
Patient sample													
DL3	1180806.8	1199134.0	1073574.75	1123297.5	1176942.1	1187060.0	311012.7	567587.1	380126.2	327761.8	396986.6	399964.5	1248989.8
DL6	1224492.38	970259.3	1064197.5	1097434.8	971074.3	1130574.4	452442.0	395559.9	403345.3	345828.5	411166.8	425813.7	492784.3
DL7	1103322.4	1119572.6	1035929.3	1113727.4	1083195.6	828673.3	629610.4	537775.9	704856.2	646716.0	710277.4	565003.7	1778047.7

C

Lymphoedema leg AT												
	# adipocyte cells						**Adipocyte size (μm^2)**					
Patient sample												
AD	87	92	124	99	102	63	5137.9	5546.8	4506.3	5646.5	6120.8	5910.7
LK	84	117	101	79	144	72	6988.4	6758.9	8012.6	5121.5	5154.3	4748.0
LS	148	165	114	127	147	99	3239.6	4012.3	3375.0	3824.1	3429.3	4510.6
MN	105	107	160	101	120	89	4999.6	4977.4	4435.9	3652.1	4655.4	3877.2

Lymphoedema leg AT													
	AT area (μm^2)						**Non-adipocyte cells (μm^2)**						**Collagen (μm^2)**
Patient sample													
AD	680508.1	1010391.5	1128849.5	935060.4	1089061.9	706309.0	230413.3	496956.1	569493.4	366567.0	459452.5	333935.7	2704460.61
LK	1031983.6	1092576.0	1129352.4	952463.6	1039383.6	963852.6	429408.4	301421.9	320081.4	538181.7	294832.2	607568.8	692776.7
LS	921215.1	1104254.5	980589.3	898427.8	1071779.5	1011376.5	440680.5	438412.5	553298.0	552624.6	408305.7	578818.4	216596.1
MN	1045845.5	1048865.0	1247685.4	1241660.8	1099632.5	1194061.9	518477.6	515091.2	535654.5	729569.1	532712.4	826226.5	305832.0

D

Normal leg AT												
	# adipocyte cells						**Adipocyte size (μm^2)**					
Patient sample												
DL1	204	152	179	167	156	176	3375.7	3991.6	3629.9	3912.9	4754.2	5021.9
DL2	186	215	183	162	233	184	3761.4	2962.5	3864.8	4138.3	3467.2	3811.8
DL4	123	152	152	118	178	157	4117.0	5191.4	4261.5	5121.1	4533.1	3166.6
DL5	153	180	175	164	162	165	2332.5	3399.9	3078.9	2825.4	4126.3	2469.5

Normal leg AT													
	AT area (μm^2)						**Non-adipocyte cells (μm^2)**						**Collagen (μm^2)**
Patient sample													
Dl1	1215210.6	1072138.9	1118454.7	1187747.8	1215552.9	1228845.6	516665.9	444886.3	466448.6	534285.4	472187.0	341527.5	767558.6
DL2	1162722.1	1122219.8	1092337.6	1172207.4	1182820.1	1142650.5	461409.2	461537.1	383024.1	494139.4	373710.1	441283.6	6671415.9
DL4	900762.9	1204185.6	1111607.0	663520.7	949906.9	1193364.0	394376.3	362482.6	418938.8	369581.2	460343.0	519504.4	4010760.2
DL5	989967.4	1077882.4	1180248.3	868969.0	1177263.1	1093802.1	596808.0	428594.3	607989.8	663261.5	422195.8	500241.3	1163604.7